Draft version April 29, 2018
Typeset using LaTeX **manuscript** style in AASTeX62

Herschel Orion Protostar Survey (HOPS) Imaging and Photometry Results.*

Babar Ali,[1] William J. Fischer,[2] S. Thomas Megeath,[3] Elise Furlan,[4] Amelia M. Stutz,[5,6] Thomas Stanke,[7] John J. Tobin,[8] James Di Francesco,[9] Lori E. Allen,[10] Dan M. Watson,[11] T. L. Wilson,[12] and Thomas Henning[5]

[1]*Space Sciences Institute, Boulder, CO, USA*

[2]*Space Telescope Science Institute, 3700 San Martin Drive, Baltimore, MD 21218, USA.*

[3]*Ritter Astrophysical Observatory, Department of Physics and Astronomy, University of Toledo, Toledo, OH, USA*

[4]*IPAC, California Institute of Technology, 1200 E. California Blvd., Pasadena, CA 91125, USA*

[5]*Max Planck Institute for Astronomy, Königstuhl 17, D-69117 Heidelberg, Germany*

[6]*Departmento de Astronomía, Facultad Ciencias Físicas y Matemáticas, Universidad de Concepción, Concepción, Chile*

[7]*European Southern Observatory, Garching bei Munchen, Germany*

[8]*Homer L. Dodge Department of Physics and Astronomy, University of Oklahoma, Norman, OK, USA*

[9]*Senior Research Officer, National Research Council Canada, Vancouver, Canada*

[10]*National Optical Astronomy Observatory, Tucson, AZ, USA*

[11]*Department of Physics and Astronomy, University of Rochester, Rochester, NY, USA*

[12]*National Science Foundation, Arlington, VA, USA*

(Received; Revised April 29, 2018; Accepted)

Submitted to ApJ

ABSTRACT

Corresponding author: Babar Ali
bali67@gmail.com

* *Herschel* is an ESA space observatory with science instruments provided by European-led Principal Investigator consortia and with important participation from NASA.

We summarize our investigation of the observed far-infrared properties of 410 protostar candidates in the Orion A and B clouds using data from the *Herschel* Space Observatory. The observations were taken as part of the Open Time Key Program *HOPS* (*Herschel* Orion Protostar Survey, PI: S. T. Megeath). The photometry portion of HOPS, discussed here, focused on 70 and 160 μm photometry with the *Herschel*/PACS instrument. This work presents our observations, data processing and map-making, and photometry analyses using both aperture and point spread function fitted photometry.

We find spatial correlations in the observed flux ratios as a function of sub-regions in both the Orion A and B clouds. Using simulations, we rule out completeness bias as the sole cause for the observed correlations. We offer differences in accretion properties and/or evolutionary status as, at least partially, responsible for the observed differences by sub-regions. Both accretion properties and evolutionary status differences, in turn, may trace fundamental differences in the star-forming conditions in the respective environments.

Keywords: stars: protostars — stars: formation — infrared: stars — submillimeter: stars

1. INTRODUCTION

A comprehensive theory of the formation of stars, which explains the origins of stars from the local raw materials and environmental conditions, is necessary for understanding processes spanning the entire range of cosmic evolution from the formation and evolution of galaxies to the formation of planets (Kennicutt & Evans 2012). Given such far-reaching significance, a primary goal of current Galactic star-formation research has been to develop such a comprehensive narrative of star formation. This importance is further underscored by the expansive open and guaranteed-time legacy-class observing programs scheduled on major space-based observatories such as *Spitzer* (Werner *et al.*

2004), and *Herschel* [1] (Pilbratt *et al.* 2010). Further, the "Birth of Stars and Protoplanetary Systems" is one of the four science themes for the James Webb Space Telescope[2].

However, many details and key ingredients are not well understood (McKee & Ostriker 2007), and are needed to complete our picture of the star formation process. In particular, one critical aspect, the connection between the raw building blocks and the conditions for star formation provided by the underlying environment and its impact on the final product (the star) is not well characterized (Dunham *et al.* 2014).

Protostars provide useful laboratories for studying the link between the local environmental conditions and the star itself. At the protostellar stage, the incipient star is still strongly connected with the local environment, and it is in the protostellar phase that the stellar mass is accumulated and protoplanetary disks are created (Evans *et al.* 2009). A detailed characterization of the protostellar evolution, thus, allows us to directly follow the evolution of raw materials.

Unfortunately, this strong link to their surroundings also makes protostars difficult to study. In particular: (i) observational studies must be able to disentangle the degenerate effects of both the environment and the star-formation process itself. Protostars are characterized by a central core, an accretion disk, outflows, and an infalling envelope (Ali *et al.* 2010). Additionally, protostars alter their local environment with phenomena such as Herbig-Haro objects (O'Dell *et al.* 1997). The spatial scales of these components range from sub-AU to 100s of AUs (McKee & Ostriker 2007). Thus, observational strategies must account for this compact, yet complicated morphology. (ii) The presence of dust in the local environment means the amount of extinction in lines-of-sight to star formation regions is abnormally high (few to several tens of magnitudes in the visual) compared to most of the rest of the Galaxy (Dobbs *et al.* 2014). Finally, (iii) *Spitzer* and *Herschel* observations, in particular, confirmed long recognized views that far-IR observations of the reprocessed radiation can probe the evolution of protostars (Adams, Lada, & Shu 1987). The presence of an infalling envelope

[1] In fact, the former name of *Herschel*, FIRST was an homage to one of primary objectives of *Herschel*: the study of the first stars and galaxies in their earliest stages.

[2] https://jwst.nasa.gov/science.html

of gas and dust is a defining characteristic of protostars. This envelope absorbs the radiation from the central accreting star+disk and reprocesses most of the luminosity into the far-IR (Ali *et al.* 2010). Far-IR observations are, therefore, absolutely crucial for efficiently identifying and studying protostars because protostars emit most of their light at those wavelengths.

The *Herschel* Orion Protostar Survey (HOPS) Open Time Key Program (PI: S. T. Megeath) was motivated by the availability of sensitive far-infrared measurements to address the challenges, (i) – (iii), mentioned above. HOPS uses a combination of strategies to mitigate these issues. First, we use multi-wavelength measurements to disentangle the protostar's components. Multi-wavelength measurements are useful because they directly connect the emergent spectral properties with the underlying physical structure and conditions of said protostar component. As these conditions vary between the components, they also vary in the emergent emission. Thus, the overall SED of the source may be modeled as the sum of contributions from the individual components (see, *e.g.*, Furlan *et al.* 2017, Ali *et al.* 2010).

Second, we focus on the nearby star-forming region, Orion (Megeath *et al.* 2012). Orion provides several key advantages. Star formation has been observed in a rich diversity of environments, from isolated cold globules to rich clusters. See, for example, Carpenter (2000), Feigelsen *et al.* (2005), Stutz *et al.* (2010). Megeath *et al.* (2012) identified a rich sample of protostars from *Spitzer* thus providing us a collection of protostars in a variety of environmental conditions. And, at 419 pc (Schlafly *et al.* 2014) , Orion is relatively nearby and, thus, affording relatively high spatial resolution to resolve morphologies.

Finally, the use of *Herschel* data, in particular, allowed us to directly measure the emission from the protostellar envelopes, and mitigate the effects of extinction. The extinction at infrared and radio wavelengths is orders of magnitude lower than at optical wavelengths (Draine 2003). The unprecedented sensitivity afforded by *Herschel* at far-infrared wavelengths allowed us to efficiently sample a large number of protostars.

This paper is one in a series describing the results from HOPS (*e.g.* Stutz *et al.* 2013, Kryukova *et al.* 2014, Fischer *et al.* 2016, Furlan *et al.* 2016). Our emphasis in this paper will be on the photometry

catalog and the observed properties of protostars. Section 2 describes our observational sample and technique. Section 3 describes our data processing and assembly of final maps. Section 4 discusses photometry of individual sources. Sections 5 & 6 present and discuss our findings. And, finally, our conclusions are summarized in Section 7.

2. PROTOSTAR SAMPLE & OBSERVATIONS

The *Spitzer* Orion protostar sample was defined and described by Megeath *et al.* (2012). For HOPS, we selected a flux-limited subset of 372 protostars for follow-up with the *Herschel* Photodetector Array Camera and Spectrometer (PACS) instrument Poglitsch *et al.* (2010). The HOPS targets are spatially spread over the Orion A and B molecular clouds from declinations of $-8°50'$ to $1°54'$ and from right ascensions of 5^h33^m to 5^h55^m. The *Herschel* observations were designed to detect those protostars with an expected 70 μm flux in excess of 42 mJy. The number of targets for the HOPS follow-up was limited solely by signal-to-noise ratio (S/N) considerations. Thirty three (33) objects in this initial list were not observed with *Herschel*. An additional four are duplicates of existing sources, in which scattered light detected with Spitzer/IRAC turned out to be associated with a nearby point source. See Furlan *et al.* (2016) for further details.

Our original sample of 372 *Herschel* targets was segregated in distinct spatial tiles to optimize observing. The tiles were assigned consecutive three-digit integer group numbers starting with the number 0 (zero). The spatial sizes of the tiles ranged from $3'$ (most common) to $7'$). The protostar candidates selected for our *Herschel* survey are referred to as the HOPS sources and are uniquely identified by a 3-digit integer number starting with the number 0 (zero). Ultimately, we detected additional 22 candidates previously identified in the *Spitzer* survey whose spatial location happened to be within the field-of-view of the observation tile. These sources, however, were not part of the original HOPS candidate list because their estimated fluxes were below our S/N limit. Further, Stutz *et al.* (2013) found protostars and candidates not identified in the *Spitzer* list; See section 2.2 for more details. Our final catalog appends the original sample of 372 targets with the additions mentioned above. There are a total of 410 sources in the final sample included here.

Furlan *et al.* (2016) classified 330 of these sources as young stellar objects (YSOs) and the remaining as unlikely to be protostars and/or sources not observed or detected by PACS at 70 micron. For their analysis, Furlan *et al.* (2016) focused on the 330 HOPS targets which have complete *Spitzer* and *Herschel* data (at least a PACS 70 μm detection) and most were originally considered protostars by Megeath *et al.* (2012). The objective of this contribution is to provide complete data on all sources from our original sample of 372 protostars as well as the additional targets detected in our images. Thus, we have included all 410 objects in this contribution.

2.1. *Observing strategy*

We used the PACS instrument (Poglitsch *et al.* 2010), and the scan-map Astronomical Observing Template (AOT) with the 20″/second scan speed for all HOPS observations. The scan map AOT offers several advantages over the point source, small source, and raster AOTs: (i) scan-map AOTs ultimately provide the best sky sampling. (ii) Scanning allows efficient mapping of groups of point-sources within individual spatial tiles. And, (iii) PACS' non-scan AOTs must employ chopping to remove background and low- frequency drifts; Chopping cannot provide optimal removal of these effects in spatially confused regions such as the protostellar fields in Orion.

We used the slowest allowed scan speed (20″/second) to avoid beam smearing and to preserve the best possible spatial resolution. By design, the PACS instrument observed both the 70 μm and 160 μm filters simultaneously. Each group of stars (spatial tile) was observed in two scan directions to avoid the so-called *striping* defect common to bolometer arrays (Tegmark 1997). These two scan directions form two distinct *Herschel* Astronomical Observing Requests (AORs). Hence, each group in our observations is assigned two separate unique identifiers, called OBSIDs. The two AORs per group are concatenated and were, therefore, assigned sequential OBSIDs. Typically, several scans are needed to cover our spatial tiles given that the size of the spatial tiles (see above) is larger than the PACS field-of-view. We allowed the PACS observing template to automatically calculate the number of scans and overlap between each scan for our required sensitivity and tile size. Our observing template observed the spatial tile with near uniform coverage.

2.2. *The observed protostar sample*

Table 1 lists the final combined catalog (see below for detailed description of columns). As noted above, in some groups, we coincidently observed additional protostars from the Megeath *et al.* (2012) *Spitzer* sample. Of note, Stutz *et al.* (2013) identified highly embedded additional protostars (the so-called PACS Bright Red Sources, PBRs). Our final catalog includes all known protostars detected by *Herschel* in the Orion fields covered by our observations.

We also investigated HOPS images for additional protostar candidates that might have been missed by our earlier efforts. Stutz *et al.* (2013) required a 160 μm detection for improved reliability, and implemented additional thresholds to reduce contamination from extra-galactic sources. As Stutz *et al.* (2013) showed, *Spitzer* observations did not identify, or in rare cases, detect all protostars in Orion. Hence, the possibility remains that additional sources, perhaps with detections only in the 70 μm filter, lurk within our data. With detection in only one or two bands, however, it is increasingly difficult to properly characterize these sources and distinguish them from foreground or background objects. It is likely necessary that additional protostar candidates here will require follow-up observations or analysis. Nonetheless, these sources may impact statistical studies, and are tabulated.

The columns have the following meaning in Table 1. Column 1 lists the unique three-digit HOPS identifier. Columns 2 & 3 list the J2000 equatorial coordinates as measured on the *Herschel* images and as reported by the DAOPHOT find algorithm (Stetson 1987). Column 4 lists the *Herschel*-assigned unique observation identifiers (OBSIDs, two per group as described in Section 2.1). Column 5 lists the 3-digit group number mentioned above. Columns 6-13 list the *Herschel* photometry for the three Herschel/PACS bands. Note these results were already reported by Furlan *et al.* (2016) and are repeated here for convenience. Our photometry procedure is described in Section 4. The 70 μm and 160 μm flux densities are from our program. The 100 μm fluxes are added from the larger survey of the Orion region from the the Gould-Belt Key Program (Konyves *et al.* 2010). The extraction of the 100μm photometry is discussed in Stutz *et al.* (2013). Each photometry value is described by three columns: the first provides the photometry value itself, the second, labelled flag, has the following

meaning: flag = 0 means the source is not observed. flag =1 means the photometry, as quoted, is the measured value, flag = 2 means the value is an upper limit, and flag=3 means the source is not detected. The third column, 'Method' identifies whether the measurement is from aperture photometry (A) or PSF-photometry (P). Column 14 identifies the sub-region within the Orion A and B clouds to which the HOPS source belongs. The sub-region definitions are listed in Table 2. Finally, Column 15 lists the Universal Time (UT) observation day for the observations. Note: when a source was detected in more than one group (tile) we combined the measurements as a simple average.

3. DATA PROCESSING & MAP-MAKING

We start data processing at the level 1 stage from the Herschel Science Archive (Wieprecht *et al.* 2009). Level 1 contains calibrated timelines[3] from individual PACS bolometers from which all instrumental effects have already been removed except for the low frequency noise component (the so-called 1/f noise[4]). Our subsequent processing mitigates the 1/f noise, combines the two independent orthogonal scan directions for each OBSID group, and projects the timelines onto the final image of the field. We will refer to these steps as 'map-making' hereafter. The processing steps leading up to level 1 are described in Poglitsch *et al.* (2010) and in the data processing guides for the Herschel Interactive Processing System, HIPE Ott *et al.* (2010). All data discussed here are based on the FM7 version of the PACS calibration (Balog *et al.* 2013) and processed with version 9 of the HIPE software. Our final maps have spatial scales of 1.6″/pixel and 3.2″/pixel for the 70 μm and 160 μm PACS filters, respectively. We used two different approaches for map-making that are described below.

3.1. *The High Pass Filter (HPF) branch*

This technique filters bolometer timelines and, as the name suggests, blocks all temporal frequencies lower than the filter width (conversely, it allows only temporal frequencies smaller than the filter

[3] Timelines are simply readouts from individual pixels ordered sequentially by time of observation. Note that for our observations the PACS instrument was used with a fixed readout frequency of 10 Hz.

[4] The so-called 1/f noise modifies the signal timelines by adding a drift component whose amplitude is a power-law function of its Fourier frequency.

width). Such filtering removes the low-frequency signal present in the timelines from both the 1/f noise as well as from astrophysical sources. The primary advantage is that point sources, whose temporal frequencies are higher than the chosen filter width, are preserved. Thus, this branch is useful for point source photometry. The HPF filtering is applied as follows: First, for any given readout in the timeline, the median value is calculated within a user-selected window of preceding and following readouts. Only those readouts that are not flagged as a glitch or otherwise identified as problematic are included in the calculation. Second, this median value is subtracted from the signal value in the current readout. The process is repeated for all readouts in the timeline. We investigated several different HPF filter window widths and settled on 15 readouts (1.5 seconds) and 20 readouts (2 seconds) for the 70 μm and 160 μm filters, respectively. These provided the optimal balance between preserving the signal from point sources and filtering out as much of the 1/f noise as possible. We use the HPF branch as implemented in HIPE and described by Popesso *et al.* (2012).

For the HPF filtering, we assume that the median value determines the local sky emission and any variations in this median value are purely due to the drift caused by 1/f noise. However, there is substantial amount of spatially extended emission in our fields from the molecular cloud itself (this emission is also referred to as nebulosity). This widespread emission has the undesired effect of altering the median values. Thus, along with the 1/f noise, the extended spatial emission (nebulosity) is also removed by the HPF processing because the value of the local sky (taken as the median, see above) includes emission from local nebulosity. In addition, point sources themselves may also elevate the median value in the HPF filter. In our map-making, we mask and exclude point sources from the median calculation. These masks are generated from the first iteration of HPF map-making and used in the 2nd iteration. We use maps only from the 2nd iteration for our analysis. We investigate the effect of nebulosity on the HPF and its consequences on the subsequent photometry in Section 4

3.2. *The Scanamorphos branch*

Scanamorphos is a map-making software developed and described by Roussel (2012). Scanamorphos removes the low-frequency noise by making use of the redundancy built in the observations. Readers are referred to Roussel (2012) for details about the processing steps. Stutz *et al.* (2013)

also used Scanamorphos-created maps for their Orion study. Unlike the HPF branch Scanamorphos preserves astrophysical emission on all spatial scales, ranging from point sources to extended structures with scales just below the map size. Scanamorphos maps are, thus, suitable for both spatially extended and point sources.

4. PHOTOMETRY

Photometry is notoriously difficult in star-forming regions. Specific challenges are: (i) differentiating spatially unresolved knots in the nebular emission from actual point sources, (ii) estimating the local background contribution. The nebular emission is usually complex and contains gradients of emission at all spatial scales that violate background homogeneity assumptions commonly used in aperture photometry and Point Spread Function (PSF)-fitted photometry algorithms. (iii) Disentangling close binaries. Further, protostars have a higher binary frequency than their main-sequence counterparts (Reipurth *et al.* 2014). We, therefore, rely on multiple approaches in both map-making and photometry to resolve these issues. The final list of photometry values is determined by combining the multiple approaches by considering the relative merits (strengths and weaknesses) of each approach for each source individually.

4.1. *Aperture photometry*

Stutz *et al.* (2013) and Furlan *et al.* (2016) describe the details of the aperture photometry procedure we followed for our images. For convenience, we briefly reprise the salient points here: We used the HPF branch images for aperture photometry measurements. To avoid nebular contamination from the local environment, we place the inner annulus of our apertures as spatially close to the source as possible. This step necessitates customized aperture corrections since the background annuli include a significant fraction of a source's point spread function (PSF) profile. We used the Vesta calibration image (PACS's PSF standard, see Lutz *et al.* 2012) to calculate aperture corrections. We set the inner radius of the sky annulus to the aperture radius to ensure the sky annulus samples the spatially varying nebulosity near the source. The adopted values for 70 μm are 9.6″, and 19.2″, for the aperture and sky outer annulus radii, respectively. The aperture correction factor is 0.7331.

In the 160 μm images, the adopted values are 12.8″, and 25.6″, for the aperture and sky annuli, respectively. The aperture correction factor at 160 μm is 0.6602.

The aperture photometry technique has several factors in its favor: First, it is a reliable and well-understood technique. Next, it is the technique used for flux calibration of the PACS instrument (Balog *et al.* 2013). Further, the use of narrow apertures as described above reduces the effect of nebular contamination and source crowding issues for most sources. However, the complex structure in the images means that brightnesses for a significant fraction of sources are not well measured using aperture photometry. The primary issue is the presence of flux from a neighboring source or strong extended emission in either the aperture or the sky annulus. The sky annulus can be particularly affected by the presence of a strong source given that we have opted to use fairly narrow sizes for them (hence, small number of pixels are available for sky estimation). These issues affect the 160 μm image more strongly because there is more extended emission detected at that wavelength. For these subset of sources, it was necessary to use a secondary photometry technique that is less susceptible to the issues noted above. The next two subsections describe our method for obtaining photometry in crowded or confused fields.

4.2. *Point Spread Function (PSF) fitted photometry*

The PSF photometry technique fits a known spatial profile for point sources to the measured point source profiles, and determines their brightnesses by the amount of scaling needed between the known and measured profiles (Stetson 1987). This scaling (hereafter referred to as the PSF amplitude) is the main quantitative measurement in this technique. The primary advantage is that the PSF-fitting technique disentangles the spatial profile of the source from other point sources and nebular contamination. Thus, it is less affected by the issues noted for aperture photometry above. This technique, however, requires that the source PSF profiles are well-characterized. Given that no clean (contamination-free) sources are available in our HOPS fields, we used the Vesta images (Lutz 2012) as proxy for the PSF profiles for our sources. We note that PACS's PSF is highly non-axisymmetric (Lutz 2012). To remove any systematical photometry offsets between PSF-based photometry and aperture-based photometry, we repeated the PSF measurements on a subset of PACS' flux standard

stars. This comparison allowed us to calibrate measured PSF amplitudes and actual flux values, as described below.

We used the *Starfinder* package (Diolaiti *et al.* 2000) for fitting PSF profiles and measuring photometry values of sources in the Scanamorphos-reduced images. The *Starfinder* source finding algorithm suffers from the same challenges as other source-finding algorithm in that many of the detected sources are unresolved compact structures in the nebular emission. We, therefore, limit our PSF-fitted photometry only to known protostars with aperture photometry issues as noted above. The remaining sources are ignored.

As mentioned earlier, the *Starfinder* PSF amplitudes must be adjusted to remove any systematic bias in PSF photometry. To that end, we processed PACS observations of flux standard stars taken in the same manner as our program stars. Then, we used *Starfinder* on these fields using exactly the same parameter set used for the HOPS program images. The measured PSF amplitudes for the flux standards and knowledge about their actual fluxes provides the necessary calibration between the two.

4.3. *Final photometry selection and errors*

When a source was observed in more than one group, we averaged the individual measurements to obtain the final estimate of its flux. We also suspected that aperture photometry results will be contaminated by the presence of other nearby sources and spatially extended nebular emission. Thus, we inspected each HOPS protostar image individually. First, visual inspection was used to identify contaminants: *e.g.* other point sources within the aperture radius, or strong nebular features that are likely to affect photometry. Once identified as problematic, we considered both PSF-fitted and aperture photometry in the context of the overall spectral energy distribution (SED) for the source. Aperture photometry for sources with strong contaminants is rejected in favor of PSF-fitted photometry. However, we opted to use the aperture photometry as an upper limit estimate of the source's flux if neither aperture, nor PSF photometry techniques yielded reliable results.

The errors for the photometry are already reported by Furlan *et al.* (2016). These were obtained as follows: (1) sources for which were observed multiple times, the error is simply 1-standard deviation

computed from all measurements. (2) Aperture photometry errors are computed at the maximum of 5% of the measured flux or the root-mean-square (RMS) variation in the intensity values within the sky annulus. And, (3) Furlan *et al.* (2016) adopted 10% of the measure flux as the error for the PSF photometry.

4.4. *100 μm photometry*

The 100 μm photometry listed in Table 1 is taken from the *Herschel* Gould Belt Survey Key Program (PI: Phillippe Andre). Stutz *et al.* (2013) describes our motivation for including the 100 μm photometry, as well the details about the photometry procedures. For the 100 μm photometry, we relied only on aperture photometry values.

5. RESULTS

In this contribution, we focus on the *observed* photometric properties of the target protostars, focusing on the fluxes in four bands: the 24 μm from *Spitzer*/MIPS and the 70, 100, and 160 μm bands from *Herschel*/PACS instruments.. A series of companion publications, Fischer *et al.* (2017), Furlan *et al.* (2016), Kryukova *et al.* (2014), and Stutz *et al.* (2013) present results and analysis from other scientific investigations and interpretations using these data from the HOPS program. Our analysis concentrates on the spatial variations in the flux and color distributions across the Orion clouds. To search for variations in the color and flux distributions, we divide the Orion clouds into 8 distinct sub-regions, shown in Table 2. We augment our analysis with previously published results for the PBR sources Stutz *et al.* (2013), and sub-mm photometry (Stanke *et al.* 2018). We present results from each of the above identified observation quantity below, and collectively discuss the implications for star-formation implied by these observations in Section 6.

5.1. *Flux distribution functions*

Figure 1 shows the flux distribution (FD) functions at 70 μm and 160 μm, respectively, for all sources detected in our sample. Figures 2 & 3 show the flux distributions segregated by sub-region, and separately for the Orion A (left column) and Orion B (right column) clouds. The sub-region and the number of associated sources are identified within the sub-panels of the Figures. We do

Table 2. The sub-region boundaries (in decimal degrees) for the Orion A & B clouds

Name	Declination Boundary		Number of protostars
	Low	High	
LDN 1622	1.3	2.08	11
NGC 2068	-0.5	1.3	59
NGC 2023/4	-3.83	-0.5	27
OMC 2/3	-5.3	-3.83	64
ONC-S	-6.1	-5.3	54
LDN 1641-N	-6.9	-6.1	47
LDN 1641-C	-7.6	-6.9	62
LDN 1641-S	-9	-7.6	85

not consider upper limits in these FDs (sources with flag value = 2 in Table 1). There are distinct differences apparent in the observed flux distributions as a function of sub-region. We note that in a flux-limited survey, such as ours, local environmental differences in the amount and structure of the nebular emission can significantly bias source detection and photometry algorithms. We quantify FD differences and investigate the role of bias below.

The 160 μm FDs show clear and obvious differences amongst the sub-regions. The following results, in particular, are noted: (i) there is a complete lack of sources below $\sim$500 mJy in OMC-2/3 region. (ii) The LDN 1641 (all) and OMC 2/3 sub-regions have apparent peaks in FDs at different flux values. (iii) The peak of the ONC-S flux distribution is between those of LDN 1641 and OMC 2/3. And, (iv) in Orion B, LDN 1622 and NGC 2023/4 show differences in the observed distribution, even with the low number of sources available.

The 160 μm FDs suggest a trend of increasingly bright sources towards lower declinations in Orion B, and increasingly bright sources towards higher declinations in Orion A. Since the sub-regions are segregated by declination in both the Orion A and B clouds, declination is a useful proxy

for sub-region. We investigate this apparent trend by plotting the median flux for each sub region as a function of declination. Figure 4 shows the resulting quantitative correlations. The median shows a systematic change as a function of declination (sub-region) as noted above. The trend is, however, weakly noted in the 70 μm fluxes, and shows OMC 2/3 region with significantly different median flux for the 160 μm fluxes. The implications for this result are discussed in Section 6.

5.2. *Flux ratio distribution*

Flux ratios (colors) are better suited for determining differences as a function of source type than the flux itself because flux ratios depend on the shape of the source SED (Ali *et al.* 2010). We investigated two different flux ratios using the combined Spitzer, HOPS and Gould-Belt photometry: $\mathrm{Log}_{10}(\lambda F_\lambda 70/\lambda F_\lambda 24)$, and $\mathrm{Log}_{10}(\lambda F_\lambda 160/\lambda F_\lambda 100)$. Figure 5 shows the flux-ratio vs flux-ratio plots segregated by sub-region for Orion A and Orion B. We do not include data with upper limits for these plots (sources with flag value = 2 in Table 1). The red symbols show the colors for the sub-region identified in the sub-panel, and the gray symbols show the colors for the entire sample. As with the median of the FD, we note an apparent systematic change in the observed flux ratios relative to the entire population in both Orion A and Orion B.

We quantitatively explore this apparent trend further in Figures 6 & 7. These Figures show the mean and median colors for each of the sub-regions as a function of the mean declination for all sources belonging to the respective sub-region.

In Orion A, the median and mean colors of the sub-regions become systematically redder towards higher declinations. In Orion B, the median and mean colors of the sub-regions becomes systematically redder towards lower declinations. For both, the vertical bar shows the 1-σ standard deviation of the flux-ratio values as a proxy for the range. Even with large variation in color, the systematic trends with declination is clearly delineated.

5.3. *Number of protostars*

Table 2 and Figure 8 list and show the numbers of HOPS protostars as a function of sub-region within the Orion A and Orion B clouds. The LDN 1641 S and C clouds have the largest number

of protostars. In Orion A, the ONC-S region has the lowest number of protostars in our *Herschel* observed sample. And, in Orion B, NGC 2068 has the largest number of protostars, more than double that of NGC 2023/2024 or LDN 1622 regions. LDN 1622 sub-region has the fewest number of protostars of all Orion sub-regions in our sample. Since the proto-stellar phase lasts <1 Myr (Megeath *et al.* 2012), the observed number of protostars may trace the sites where recent star-formation are transpiring. We note, however, that Stutz *et al.* (2013) find that Orion B, which has the fewest protostars, have the most PBRs, suggesting youth.

6. DISCUSSION

The results presented in Section 5 show the global properties of the HOPS protostar sample. Since the sub-regions in Orion A and B are well stratified by declination, differences are easily explored by using declination as a proxy for sub-region. Indeed, Figures 4, 6, & 7 show that systematic variations exist in the observed proto-stellar properties as a function of declination in the Orion A & B clouds. **We discuss in Sections 6.1 & 6.2 two explanations of this observed trend. Again, we will restrict ourselves to observed quantities only and leave the detailed exploration of inferred properties to companion papers. We rule out inclination angle (to the observer) as a factor because no reasonable justification can be made for systematic differences in inclination as a function of sub-region in Orion.**

6.1. *Completeness limit bias*

Here, we discuss whether photometric completion limit biases our observations and produces the apparent trends discussed above. Completeness limits are difficult to estimate accurately. The detection efficiency is a strong function of the magnitude of the local nebular emission; Hence, we expect the limits to vary considerably even within a single sub-region as the nebular emission itself varies inside any of our adopted sub-region boundaries. This variation makes it difficult to disentangle observational bias from any real trends shown in Figures 4, & 5.

Fortunately, there is a way to decouple detection bias. Differences in completeness limit will affect the median flux distribution (Figure 4), since such differences will bias the median calculation. For

the same effect to exist also in the flux ratio correlation (Figure 5) requires that the observed flux be correlated with flux ratio. We investigate this possibility by directly examining the data for such a correlation, and via a simple simulation described below.

Figure 9 shows the observed 70 μm flux as a function of the flux ratios used in our investigation. We note a marginal dependence of 70 μm flux with the $\mathrm{Log}_{10}(\lambda F_\lambda 70/\lambda F_\lambda 24)$ color, and no obvious correlation with $\mathrm{Log}_{10}(\lambda F_\lambda 160/\lambda F_\lambda 100)$. The first trend is not surprising because the protostar flux is dominated by the envelope whose SED peaks near 70 μm. Indeed, 70 μm flux changes likely track changes in the amount of material present in the envelope. In addition, material deeper inside the envelope (closer to the protostar) will be warmer and, hence, will emit more brightly at 70 μm than at 100 μm or 160 μm. Therefore, we expect to notice the equivalent of a hotter black body with lesser envelope material. The $\mathrm{Log}_{10}(\lambda F_\lambda 160/\lambda F_\lambda 100)$ color samples the Rayleigh-Jeans side of the SED peak and should show only marginal variation with changing temperature. On the other hand, the $\mathrm{Log}_{10}(\lambda F_\lambda 70/\lambda F_\lambda 24)$ color samples the Wien side of the SED and is more likely to show some variation. Following this reasoning, we understand the loose correlation seen only between 70 μm flux and $\mathrm{Log}_{10}(\lambda F_\lambda 70/\lambda F_\lambda 24)$ in Figure 9. However, we note that the $\mathrm{Log}_{10}(\lambda F_\lambda 70/\lambda F_\lambda 24)$ is also influenced by inclination and cavity geometry, which can creates additional spread in said color ratio.

We can now further investigate completeness limit and observational bias via a simple simulation. The LDN 1641 sub-regions contain the largest number of protostars (see Table 2) and visual inspection shows the least contamination of the sample from extended nebulosity. Further, fainter protostars are detected in LDN 1641 than in Orion OMC 2/3. Hence, if bright, complex, spatially extended emission from the local dust is responsible for decreased reliability and higher completeness limits for point source photometry, then LDN 1641 provides an ideal contrast to the Orion OMC 2/3 sub-region. The contrast between LDN 1641 and Orion OMC-2/3 is at the extreme ends of the spatial correlation observed in Figures 4 & 5.

We can simulate the bias introduced by completeness limit for OMC-2/3 by restricting the observed fluxes in LDN 1641 to only those protostars that are above a simulated completeness limit and recomputing statistical averages. We require that the population of protostars be fundamentally

the same between OMC-2/3 and LDN 1641. If this assumption is not valid, then actual population differences must exist between the two sub-regions. (This scenario is discussed below in Section 6.2). We then re-calculate the mean color of LDN 1641 from the restricted sample. Figure 10 shows the result of our simulation on a plot of median flux ratio vs the completeness limit for LDN 1641 (solid line) and Orion OMC-2/3 region (dashed line). The top panel shows the results for median $\mathrm{Log}_{10}(\lambda F_\lambda 70/\lambda F_\lambda 24)$, and the bottom panel for median $\mathrm{Log}_{10}(\lambda F_\lambda 160/\lambda F_\lambda 100)$.

The median flux ratio, $\mathrm{Log}_{10}(\lambda F_\lambda 160/\lambda F_\lambda 100)$, in Figure 10 (bottom panel) remains nearly constant as the simulated completeness limit is increased. **We conclude that observational bias cannot explain the correlation seen in Figure 7**. On the other hand, observational bias does become significant for $\mathrm{Log}_{10}(\lambda F_\lambda 70/\lambda F_\lambda 24)$ when the completeness limit is near 0.5 Janskys. These conclusions support the results shown in Figure 9 that 70 μm flux is correlated with $\mathrm{Log}_{10}(\lambda F_\lambda 70/\lambda F_\lambda 24)$, but not with $\mathrm{Log}_{10}(\lambda F_\lambda 160/\lambda F_\lambda 100)$. Actual population differences between the sub-regions, however, cannot be ruled out. In the absence of completeness bias for $\mathrm{Log}_{10}(\lambda F_\lambda 160/\lambda F_\lambda 100)$, it is difficult to explain how the correlation in Figure 7 does not reflect actual differences in the underlying populations. $\mathrm{Log}_{10}(\lambda F_\lambda 160/\lambda F_\lambda 100)$is insensitive to extinction and directly measures the reprocessed light from protostellar envelopes. We postulate that because actual population differences are impossible to rule out for $\mathrm{Log}_{10}(\lambda F_\lambda 160/\lambda F_\lambda 100)$, then the changes in flux ratio with declination shown in Figure 6 must at least partially reflect real population differences between the sub-regions.

6.2. *Population differences*

We also consider systematic differences in the underlying protostar population as a possible cause for the observed correlations in Figures 6 & 7. Fischer *et al.* (2017) provide observational evidence for such a scenario. Fischer *et al.* (2017) derived bolometric luminosities and temperatures of our HOPS protostar sample and find statistical differences in the bolometric properties of the protostars as a function of the sub-region in Orion A and B clouds. The authors argue that these differences track an underlying difference in the star-formation rate across the sub-regions leading to a different mixture of protostars and more evolved objects. Their findings are supported, in part, by

evidence that the fractions for both Class 0 stars and PBRs compared to Class I and II objects are also different in the subregions (Stutz *et al.* 2013).

Ali *et al.* (2010) find protostellar envelopes to be the dominant factor affecting the observed colors in the *Herschel* bands. Given that large, active envelopes are the defining characteristics of Class 0 objects and PBRs, the correlations apparent in Figures 6 & 7 are consistent with the population differences suggested by Fischer *et al.* (2017) and Stutz *et al.* (2013). Our data is insufficient to establish causal links for said envelope differences. However, when taken together, these results support a scenario of systematic differences in the age and/or local environment within the Orion A & B clouds with the ONC sub-region undergoing the most recent episode of increased star formation or a ramping up of the star formation rate.

Alternatively, changing the size and/or shape of the outflow cavities may also affect the observed *Herschel* colors by allowing more radiation to escape and by the contribution of the warm cavity walls. We can similarly identify other proto-stellar model parameters investigated by Ali *et al.* (2010) to produce the observed color differences. We still favor differences in envelopes properties because, as stated earlier, envelopes are the strongest influencers on *Herschel* colors (Ali *et al.* 2010).

7. CONCLUSIONS

We explored the mid- to far-infrared properties of the Orion protostars obtained as part of the *Herschel*Key Program HOPS. Investigations of the observed properties of these protostars reveal apparent correlations as a function of sub-regions in both the Orion A and B clouds. We investigated the role of bias introduced due to differences in completeness limits in these correlations by artificially introducing a completeness limit in the LDN 1641 sub-region and comparing the resulting changes in median flux ratio to Orion OMC-2/3 values. These simulations suggest that completeness limit bias alone is not sufficient to explain the observed correlation for $\mathrm{Log}_{10}(\lambda F_\lambda 160/\lambda F_\lambda 100)$.

An alternative explanation may be population differences between these sub-regions. **In particular, we find that systematic differences in protostellar envelope densities (correlating**

with their size and color, see Ali *et al.* 2010) are consistent with population differences suggested by Fischer *et al.* (2017) and Stutz *et al.* (2013). In this scenario, we favor the interpretation that *Herschel* colors are influenced by protostellar envelopes over other factors because Ali *et al.* (2010) find envelopes as the strongest protostellar feature affecting their *Herschel* colors. Further, this scenario implies that said differences in envelope properties and protostars are likely from differences in the age or the local star-formation environment. We cannot further differentiate whether evolution or the environment led to such a difference in the protostars. For example, denser regions may systematically produce denser envelopes which collapse with higher infall rates and may resemble envelopes from a more evolved population with lower density.

BA was partially supported with NASA grant IPAC.ALI-OTKP-1-JPL.000094 for this work.

The work of AMS was partially supported by the Deutsche Forschungsgemeinschaft priority program 1573 ("Physics of the Interstellar Medium").

J. Tobin acknowledges support provided by NASA through Hubble Fellowship grant HST-HF-51300.01-A awarded by the Space Telescope Science Institute, which is operated by the Association of Universities for Research in Astronomy, Inc., for NASA, under contract NAS 5-26555. The National Radio Astronomy Observatory is a facility of the National Science Foundation operated under cooperative agreement by Associated Universities, Inc.

The Herschel spacecraft was designed, built, tested, and launched under a contract to ESA managed by the Herschel/Planck Project team by an industrial consortium under the overall responsibility of the prime contractor Thales Alenia Space (Cannes), and including Astrium (Friedrichshafen) responsible for the payload module and for system testing at spacecraft level, Thales Alenia Space (Turin) responsible for the service module, and Astrium (Toulouse) responsible for the telescope, with in excess of a hundred subcontractors.

PACS has been developed by a consortium of institutes led by MPE (Germany) and including UVIE (Austria); KU Leuven, CSL, IMEC (Belgium); CEA, LAM (France); MPIA (Germany); INAF-

IFSI/OAA/OAP/OAT, LENS, SISSA (Italy); IAC (Spain). This development has been supported by the funding agencies BMVIT (Austria), ESA-PRODEX (Belgium), CEA/CNES (France), DLR (Germany), ASI/INAF (Italy), and CICYT/MCYT (Spain).

HIPE is a joint development by the Herschel Science Ground Segment Consortium, consisting of ESA, the NASA Herschel Science Center, and the HIFI, PACS and SPIRE consortia.

Facilities:

Facility: Herschel Space Observatory (PACS)

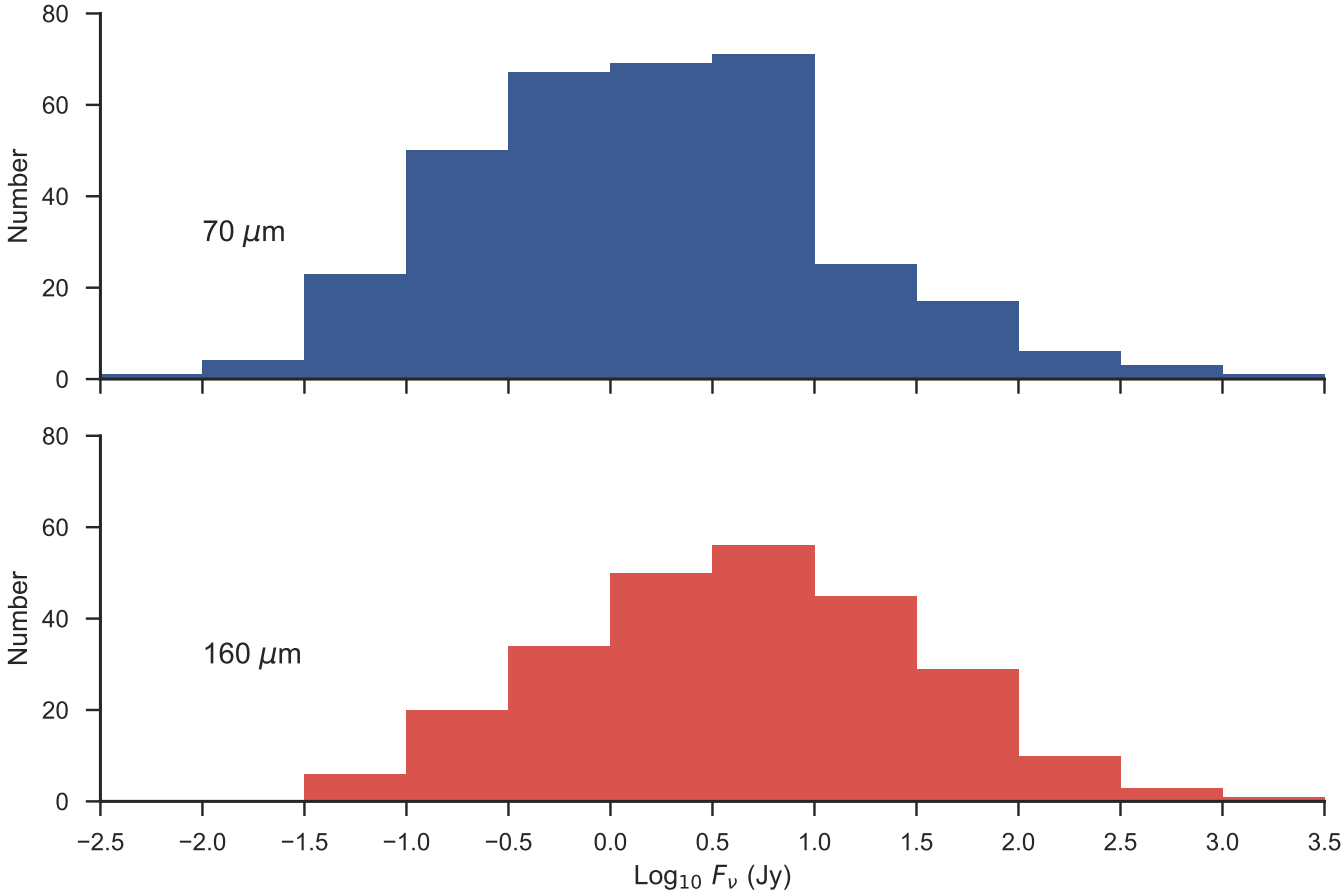

Figure 1. Flux distributions at 70 μm (top, blue) and 160 μm (bottom, red) for all sources in the HOPS sample. Only sources with actual measurements are shown. The upper limits are not used.

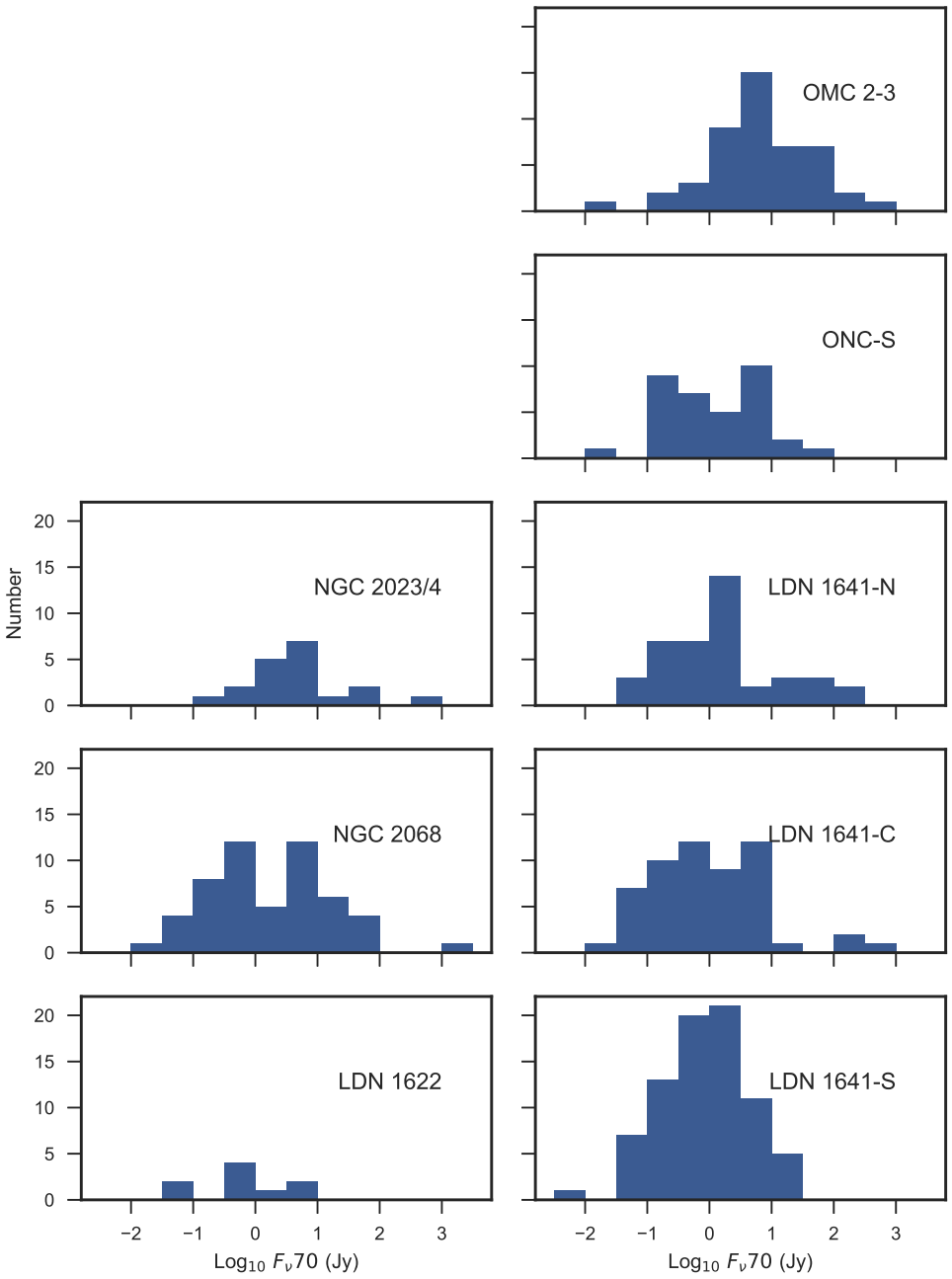

Figure 2. The 70 μm flux distributions segregated by sub-region for Orion B (left column) and Orion A (right column).

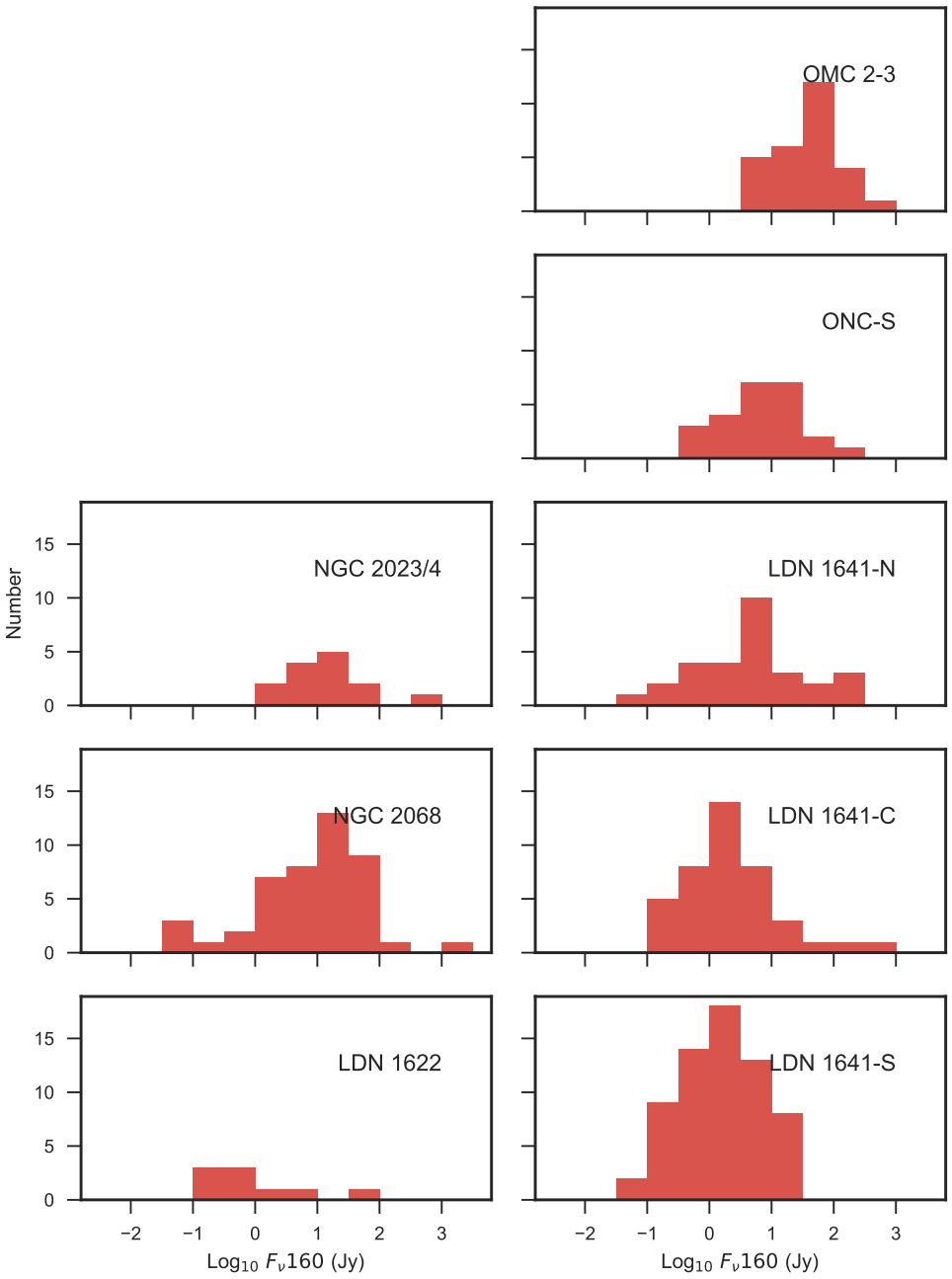

Figure 3. The 160 μm flux distributions segregated by subregion for Orion B (left column) and Orion A (right column).

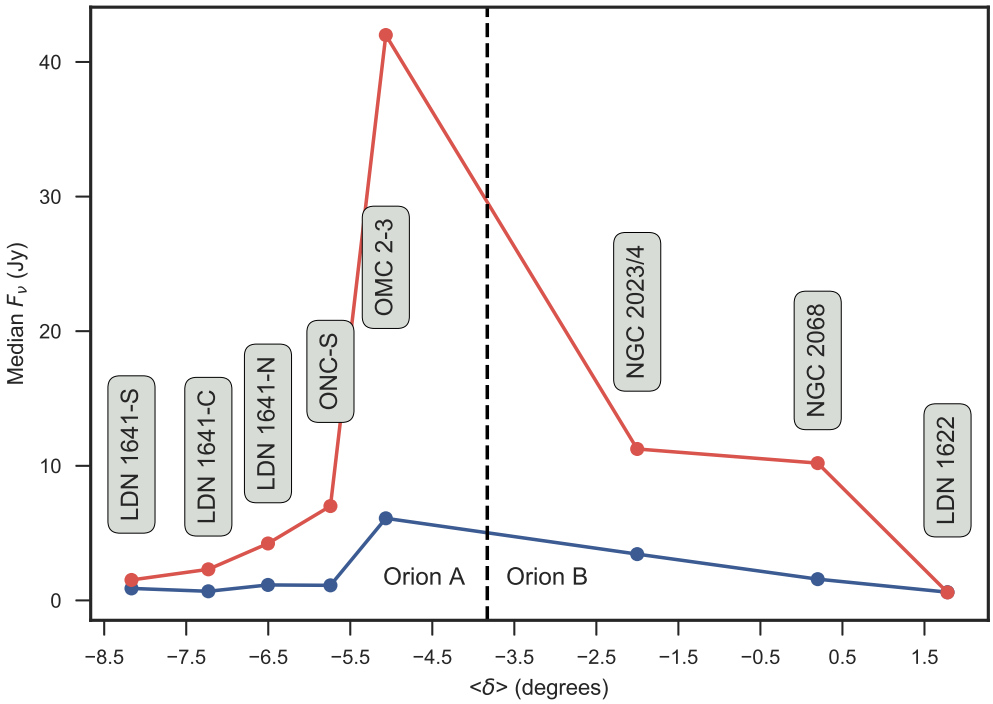

Figure 4. Median flux as a function of declination for the 70 μm FD (blue dots and curve) and the 160 μm FD (red dots and curve).

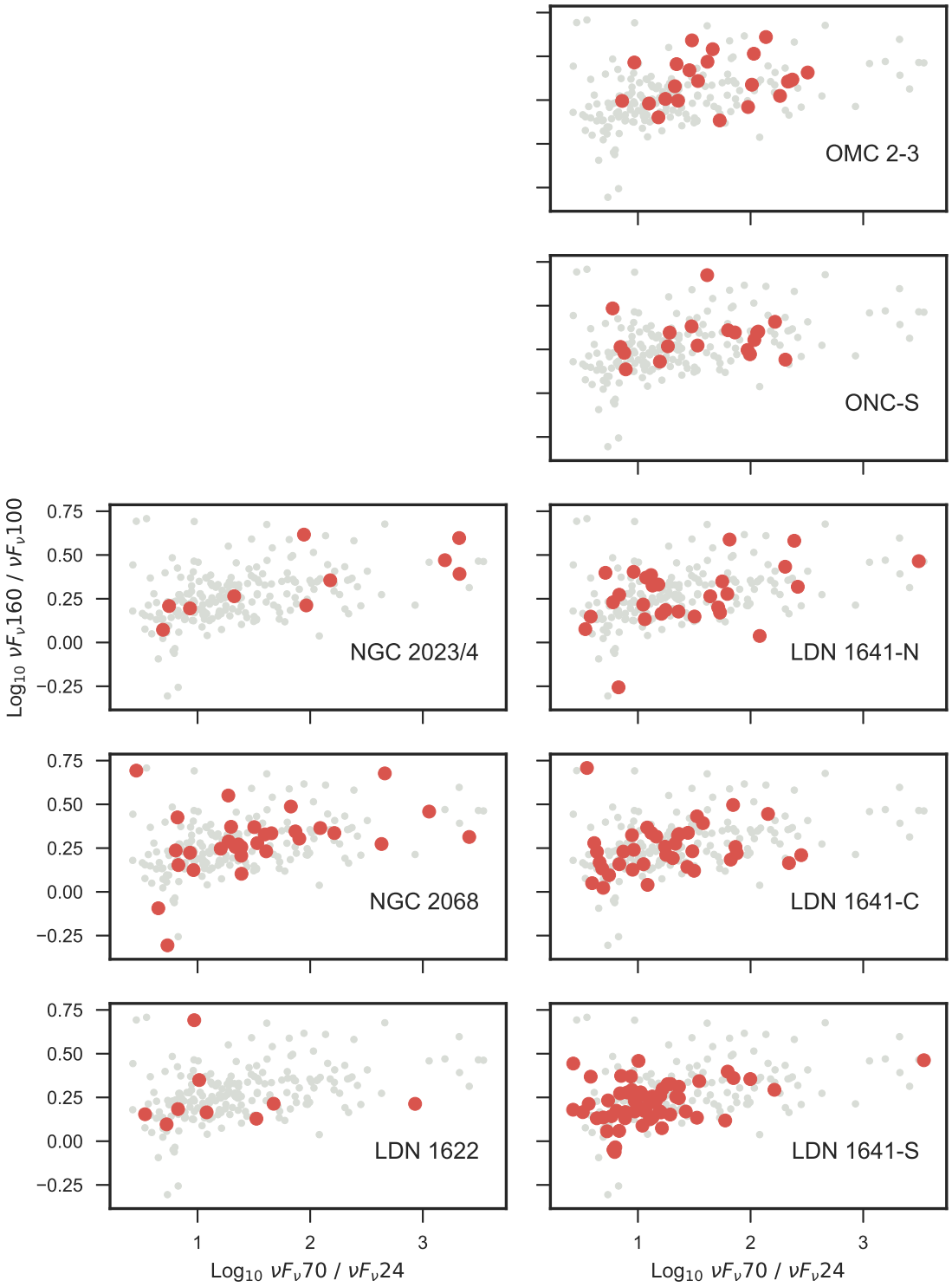

Figure 5. The observed distribution of colors in Orion A (right panel) and Orion B (left panel) segregated by sub-regions. The sub-region is identified in each respective panel. Solid red symbols show the colors for the sub-region. Small grey symbols show the distribution for all sources in the combined Orion A and Orion B samples.

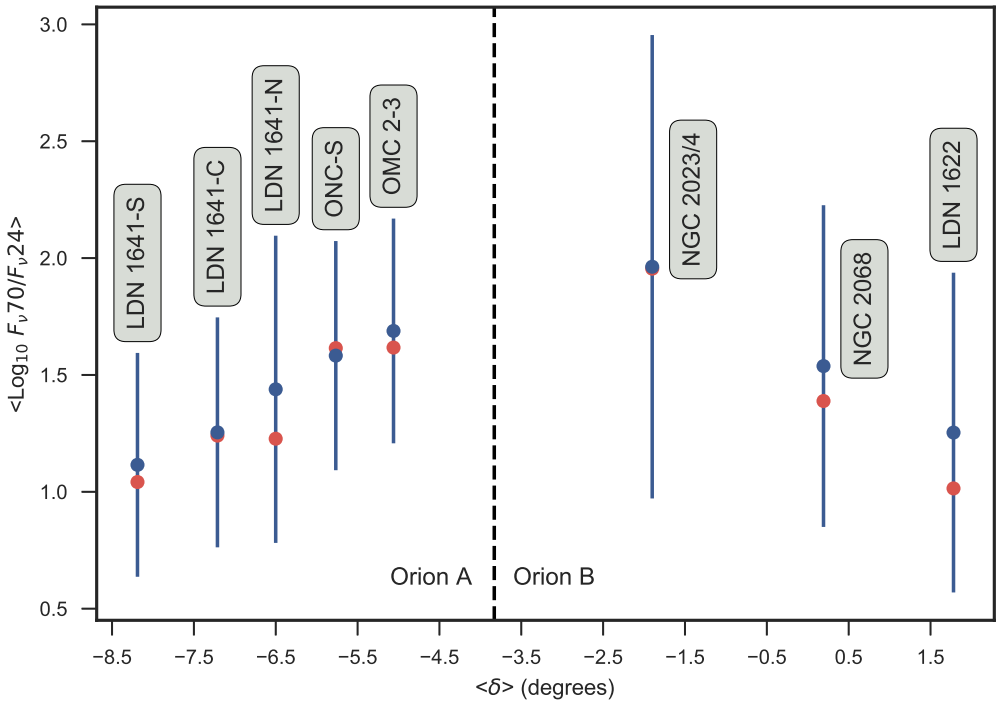

Figure 6. The mean (blue circles) and median (red circles) value of $\mathrm{Log}_{10}(\lambda F_\lambda 70/\lambda F_\lambda 24)$ color as a function of declination. The associated sub-region is labelled above the data points themselves. The vertical bars show the respective standard deviation.

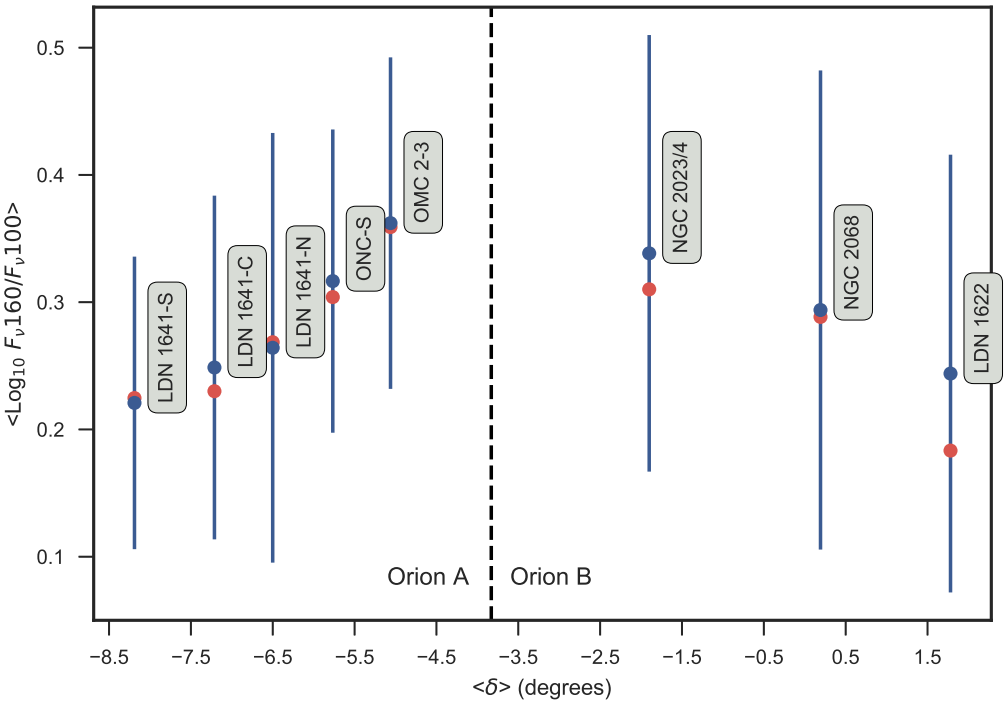

Figure 7. Same as Figure 6 for the $\mathrm{Log}_{10}(\lambda F_\lambda 160/\lambda F_\lambda 100)$ color.

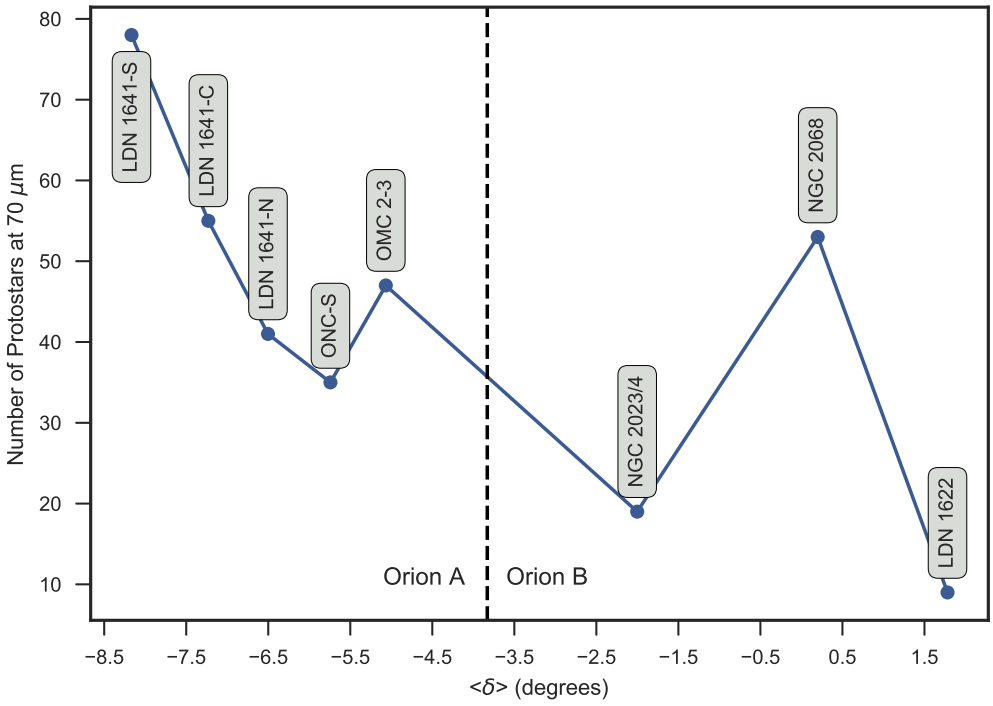

Figure 8. The number of protostars as a function of sub-region in Orion.

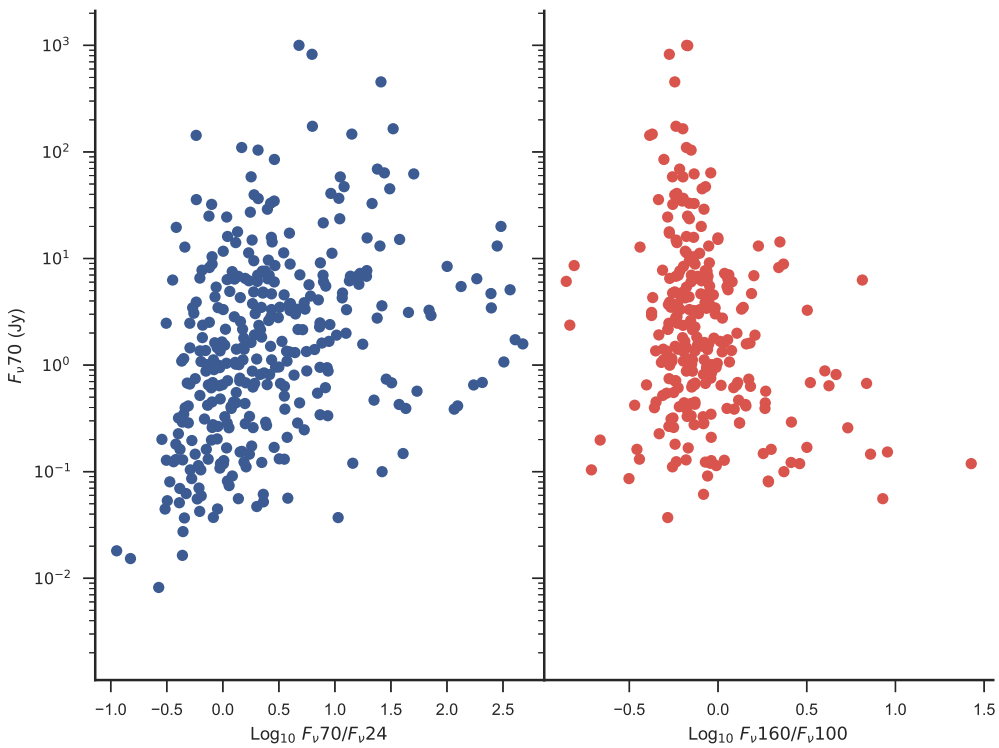

Figure 9. Flux density vs log flux ratio diagrams for Orion. (left) The observed 70 μm flux as a function of the $\mathrm{Log}_{10}(\lambda F_\lambda 70/\lambda F_\lambda 24)$, and $\mathrm{Log}_{10}(\lambda F_\lambda 160/\lambda F_\lambda 100)$ (right) flux ratios.

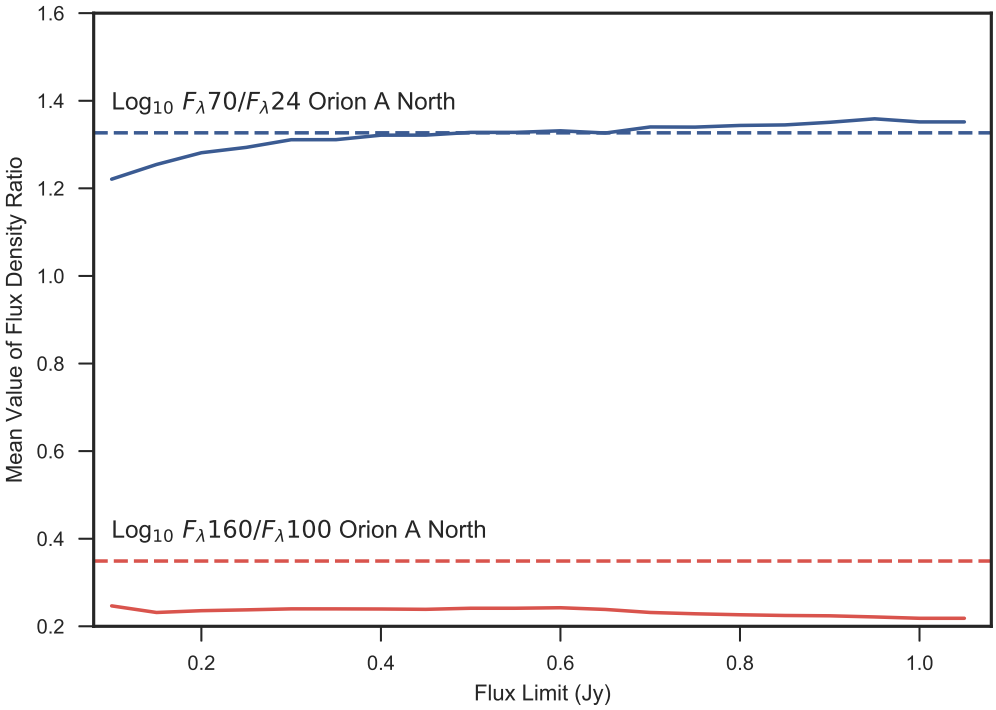

Figure 10. Completion limit as an explanation for observed color differences in the Orion sub-regions. The observed mean color above the artificially imposed completeness limit for LDN 1641. Solid lines show the mean values for $\mathrm{Log}_{10}(\lambda F_\lambda 70/\lambda F_\lambda 24)$ (blue) and $\mathrm{Log}_{10}(\lambda F_\lambda 160/\lambda F_\lambda 100)$ (red) with the chosen limiting flux. The dashed lines show the mean color for the combined Orion ONC and OMC-2/3 region. As discussed in text, we note a complete lack of correlation between the artificially imposed completeness limit and mean color for $\mathrm{Log}_{10}(\lambda F_\lambda 160/\lambda F_\lambda 100)$. We note a steady increase in the mean $\mathrm{Log}_{10}(\lambda F_\lambda 70/\lambda F_\lambda 24)$as a function of the completeness limit. Differences in $\mathrm{Log}_{10}(\lambda F_\lambda 70/\lambda F_\lambda 24)$ between LDN-1641 and Orion OMC-2/3 + ONC can be explained as difference in completions limits. However, completion limit differences cannot explain the color differences for $\mathrm{Log}_{10}(\lambda F_\lambda 160/\lambda F_\lambda 100)$ in these simulations for the sub-regions.

APPENDIX

A. HOPS CATALOG

The HOPS observational catalog.

Table 1. The HOPS observation sample

HOPS	α_{J2000}	δ_{J2000}	OBSID[a]	Group	70μm	flag[b]	Method[c]	100μm	flag[b]	160μm	flag[b]	Method[c]	Field	Observation Date
	h:m:s	^{o} :$'$:$''$			(mJy)			(mJy)		(mJy)				(UT)
(1)	(2)	(3)	(4)	(5)	(6)	(7)	(8)	(9)	(10)	(11)	(12)	(13)	(14)	(15)
000	05:54:28.11	01:37:34.9	···	···	···	0	A	···	3	···	0	A	···	···
001	05:54:12.34	01:42:35.5	1342215365-66	000	3.700	1	A	4.570	1	3.840	1	A	LDN 1622	6 Mar 2011
002	05:54:9.13	01:42:52.0	1342215365-66	000	0.519	1	A	0.514	1	0.401	1	P	LDN 1622	6 Mar 2011
003	05:54:56.97	01:42:56.2	1342218780-81	001	0.319	1	A	0.294	1	0.262	1	A	LDN 1622	18 Apr 2011
004	05:54:53.76	01:47:10.0	1342218780-81	001	0.612	1	A	0.622	1	0.593	1	A	LDN 1622	18 Apr 2011
005	05:54:32.16	01:48:7.2	1342218703-04	003	0.710	1	A	0.753	1	0.688	1	A	LDN 1622	16 Apr 2011
006	05:54:18.41	01:49:3.4	1342218703-04	003	0.091	1	A	0.136	1	0.190	1	A	LDN 1622	16 Apr 2011
007	05:54:20.04	01:50:42.8	1342218703-04	003	1.340	1	A	1.750	1	1.790	1	A	LDN 1622	16 Apr 2011
008	05:35:33.11	-05:59:6.4	1342227328-29	006	···	3	A	···	3	···	3	A	ONC-S	24 Aug 2011
009	05:35:49.21	-05:59:3.6	···	···	···	0	A	···	3	···	0	A	···	···
010	05:35:9.00	-05:58:27.6	1342204248-49	005	6.820	1	A	12.600	1	17.700	1	A	ONC-S	9 Sep 2010
011	05:35:13.41	-05:57:58.1	1342204248-49	005	23.600	1	A	33.000	1	36.400	1	A	ONC-S	9 Sep 2010
012	05:35:8.60	-05:55:54.3	1342204248-49	005	15.600	1	A	26.100	1	41.700	1	P	ONC-S	9 Sep 2010
013	05:35:24.56	-05:55:33.4	1342227328-29	006	1.120	1	A	0.932	1	1.070	1	A	ONC-S	24 Aug 2011
014	05:36:19.17	-05:55:30.3	1342227326-27	007	···	3	A	···	3	3.630	2	A	ONC-S	24 Aug 2011
015	05:36:19.02	-05:55:25.5	1342227326-27	007	0.258	1	A	0.340	1	2.930	2	A	ONC-S	24 Aug 2011
016	05:35:0.81	-05:55:25.7	1342204248-49	005	0.685	1	A	1.220	1	6.470	2	A	ONC-S	9 Sep 2010
017	05:35:7.18	-05:52:5.9	1342217446-47	008	0.673	1	A	0.541	1	5.950	2	A	ONC-S	30 Mar 2011
018	05:35:5.49	-05:51:54.4	1342217446-47	008	4.270	1	A	6.050	1	6.310	1	P	ONC-S	30 Mar 2011
019	05:35:25.99	-05:51:22.9	1342217446-47	008	0.247	1	A	···	3	0.953	1	P	ONC-S	30 Mar 2011

Table 1 continued on next page

Table 1 *(continued)*

HOPS	α_{J2000}	δ_{J2000}	OBSID[a]	Group	70μm	flag[b]	Method[c]	100μm	flag[b]	160μm	flag[b]	Method[c]	Field	Observation Date
	h:m:s	^{o} :$'$:$''$			(mJy)			(mJy)		(mJy)				(UT)
(1)	(2)	(3)	(4)	(5)	(6)	(7)	(8)	(9)	(10)	(11)	(12)	(13)	(14)	(15)
020	05:33:30.71	-05:50:41.0	1342217750-51	009	1.370	1	A	1.710	1	3.260	1	A	ONC-S	31 Mar 2011
021	05:36:10.10	-05:50:8.3	1342227096-97	010	0.119	1	A	0.299	2	1.380	2	A	ONC-S	22 Aug 2011
022	05:35:0.53	-05:49:2.0	1342217446-47	008	0.146	1	A	0.550	2	6.370	2	A	ONC-S	30 Mar 2011
023	05:36:17.89	-05:46:54.5	1342227096-97	010	···	3	A	···	3	···	3	A	ONC-S	22 Aug 2011
024	05:34:46.94	-05:44:51.0	1342204246-47	012	0.291	1	A	···	3	0.581	2	A	ONC-S	9 Sep 2010
025	05:35:22.63	-05:44:29.5	1342227098-99	013	···	3	A	···	3	···	3	A	ONC-S	22 Aug 2011
026	05:35:17.34	-05:42:14.5	1342227098-99	013	0.130	1	A	···	3	2.300	2	A	ONC-S	22 Aug 2011
027	05:36:21.72	-05:41:58.1	···	···	···	0	A	0.493	1	···	0	A	···	···
028	05:34:47.29	-05:41:55.9	1342204246-47	012	0.945	1	A	1.850	1	2.570	1	P	ONC-S	9 Sep 2010
029	05:34:49.04	-05:41:42.2	1342204246-47	012	3.770	1	A	4.120	1	3.900	1	P	ONC-S	9 Sep 2010
030	05:34:44.06	-05:41:25.9	1342204246-47	012	7.610	1	A	9.370	1	13.000	1	P	ONC-S	9 Sep 2010
031	05:35:17.25	-05:40:26.9	1342227098-99	013	···	3	A	···	3	···	3	A	ONC-S	22 Aug 2011
032	05:34:35.45	-05:39:59.1	1342204244-45	014	6.170	1	A	5.550	1	7.710	1	P	ONC-S	9 Sep 2010
033	05:34:45.21	-05:39:56.8	1342204246-47	012	0.108	1	A	···	3	0.751	2	A	ONC-S	9 Sep 2010
034	05:35:10.90	-05:39:30.7	1342205234-35	015	···	3	A	···	3	···	3	A	ONC-S	28 Sep 2010
035	05:35:19.93	-05:39:1.2	1342205234-35	015	···	3	A	···	3	···	3	A	ONC-S	28 Sep 2010
036	05:34:26.43	-05:37:40.5	1342204244-45	014	0.997	1	A	1.020	1	0.872	1	A	ONC-S	9 Sep 2010
037	05:34:47.67	-05:37:25.2	1342204244-45	014	···	3	A	···	3	···	3	A	ONC-S	9 Sep 2010
038	05:35:4.72	-05:37:12.3	1342205234-35	015	0.272	1	P	···	3	17.000	2	A	ONC-S	28 Sep 2010
039	05:36:22.43	-05:36:24.8	···	···	···	0	A	0.445	1	···	0	A	···	···
040	05:35:8.52	-05:35:59.4	1342205234-35	015	3.310	1	A	11.600	1	14.600	1	P	ONC-S	28 Sep 2010
041	05:34:29.44	-05:35:42.7	1342204244-45	014	4.560	1	A	7.040	1	10.600	1	A	ONC-S	9 Sep 2010
042	05:35:5.04	-05:35:40.7	1342205234-35	015	1.310	1	A	···	3	28.800	2	A	ONC-S	28 Sep 2010

Table 1 continued on next page

Table 1 *(continued)*

HOPS	α_{J2000}	δ_{J2000}	OBSID[a]	Group	70μm	flag[b]	Method[c]	100μm	flag[b]	160μm	flag[b]	Method[c]	Field	Observation Date
	h:m:s	^{o} :$'$:$''$			(mJy)			(mJy)		(mJy)				(UT)
(1)	(2)	(3)	(4)	(5)	(6)	(7)	(8)	(9)	(10)	(11)	(12)	(13)	(14)	(15)
043	05:35:4.50	-05:35:14.4	1342205234-35	015	3.250	1	P	14.700	1	17.200	1	P	ONC-S	28 Sep 2010
044	05:35:10.57	-05:35:6.3	1342205234-35	015	0.956	1	P	···	3	13.000	1	A	ONC-S	28 Sep 2010
045	05:35:6.45	-05:33:35.1	1342205234-35	015	6.550	1	P	···	3	8.530	1	A	ONC-S	28 Sep 2010
046	05:34:42.20	-05:33:3.3	1342217448-49	016	···	3	A	···	3	6.330	2	A	ONC-S	30 Mar 2011
047	05:33:45.87	-05:32:58.1	1342204433-34	308	0.018	1	A	···	3	0.490	2	A	ONC-S	13 Sep 2010
048	05:35:6.56	-05:32:51.6	1342205234-35	015	5.670	2	A	···	3	···	3	A	ONC-S	28 Sep 2010
049	05:34:48.88	-05:31:45.9	1342217448-49	016	0.664	1	A	···	3	0.622	2	A	ONC-S	30 Mar 2011
050	05:34:40.91	-05:31:44.4	1342217448-49	016	9.110	1	A	14.200	1	20.300	1	A	ONC-S	30 Mar 2011
051	05:35:15.83	-05:30:5.5	1342217450-51	017	···	3	A	···	3	···	3	A	ONC-S	30 Mar 2011
052	05:35:16.32	-05:29:32.6	1342217450-51	017	···	3	A	···	3	···	3	A	ONC-S	30 Mar 2011
053	05:33:57.37	-05:23:30.4	1342217752-53	018	69.000	1	A	106.000	1	103.000	1	A	ONC-S	31 Mar 2011
054	05:33:22.48	-05:23:2.9	···	···	···	0	A	···	3	···	0	A	···	···
055	05:33:54.09	-05:21:49.5	1342217752-53	018	···	3	A	···	3	1.230	1	A	ONC-S	31 Mar 2011
056	05:35:19.47	-05:15:32.7	1342205232-33	200	47.200	1	A	94.100	1	128.000	1	P	OMC 2-3	28 Sep 2010
057	05:35:19.84	-05:15:8.5	1342205232-33	200	4.910	1	A	···	3	75.100	2	A	OMC 2-3	28 Sep 2010
058	05:35:18.51	-05:13:38.2	1342205232-33	200	3.460	1	A	···	3	3.810	2	A	OMC 2-3	28 Sep 2010
059	05:35:20.14	-05:13:15.5	1342205232-33	200	58.400	1	A	65.600	1	58.100	1	P	OMC 2-3	28 Sep 2010
060	05:35:23.33	-05:12:3.1	1342205228-29	130	58.300	1	A	83.400	1	84.600	1	A	OMC 2-3	28 Sep 2010
061	05:33:25.91	-05:12:2.6	···	···	···	0	A	···	3	···	0	A	···	···
062	05:35:24.58	-05:11:29.7	1342205228-29	130	···	3	A	···	3	44.000	2	A	OMC 2-3	28 Sep 2010
063	05:35:24.90	-05:10:1.5	1342205228-29	130	···	3	A	···	3	···	3	A	OMC 2-3	28 Sep 2010
064	05:35:27.00	-05:09:54.1	1342205228-29	130	···	3	A	···	3	···	3	A	OMC 2-3	28 Sep 2010
065	05:35:21.55	-05:09:38.7	1342205228-29	130	0.481	1	A	···	3	28.400	2	A	OMC 2-3	28 Sep 2010

Table 1 continued on next page

Table 1 *(continued)*

HOPS	α_{J2000}	δ_{J2000}	OBSID[a]	Group	70μm	flag[b]	Method[c]	100μm	flag[b]	160μm	flag[b]	Method[c]	Field	Observation Date
	h:m:s	^{o} :$'$:$''$			(mJy)			(mJy)		(mJy)				(UT)
(1)	(2)	(3)	(4)	(5)	(6)	(7)	(8)	(9)	(10)	(11)	(12)	(13)	(14)	(15)
066	05:35:26.84	-05:09:24.6	1342205228-29	130	27.200	1	P	···	3	325.000	2	A	OMC 2-3	28 Sep 2010
067	05:35:22.69	-05:08:34.0	1342205228-29	130	···	3	A	···	3	···	3	A	OMC 2-3	28 Sep 2010
068	05:35:24.30	-05:08:30.6	1342205228-29	130	6.960	1	A	14.300	1	25.500	1	A	OMC 2-3	28 Sep 2010
069	05:35:25.22	-05:08:24.0	1342205228-29	130	···	3	A	···	3	15.600	2	A	OMC 2-3	28 Sep 2010
070	05:35:22.41	-05:08:4.8	1342205228-29	130	6.410	1	P	···	3	11.600	1	A	OMC 2-3	28 Sep 2010
071	05:35:25.61	-05:07:57.3	1342205228-29	130	14.300	1	A	13.100	1	46.800	2	A	OMC 2-3	28 Sep 2010
072	05:35:25.71	-05:07:46.4	1342205228-29	130	···	3	A	···	3	···	3	A	OMC 2-3	28 Sep 2010
073	05:35:27.70	-05:07:3.5	1342205226-27	135	1.670	1	A	7.110	1	11.700	1	A	OMC 2-3	28 Sep 2010
074	05:35:24.86	-05:06:21.4	1342205228-29	130	1.010	1	A	···	3	23.800	2	A	OMC 2-3	28 Sep 2010
075	05:35:26.66	-05:06:10.3	1342205226-27	135	7.030	1	A	11.900	1	21.900	1	P	OMC 2-3	28 Sep 2010
076	05:35:25.75	-05:05:57.9	1342205226-27	135	2.160	1	P	···	3	9.740	1	A	OMC 2-3	28 Sep 2010
077	05:35:31.53	-05:05:47.3	1342205226-27	135	8.870	1	A	9.090	1	34.000	2	A	OMC 2-3	28 Sep 2010
078	05:35:25.82	-05:05:43.7	1342205226-27	135	15.100	1	A	35.500	1	56.700	1	P	OMC 2-3	28 Sep 2010
079	05:35:27.88	-05:05:36.3	1342205228-29	130	···	3	A	···	3	···	3	A	OMC 2-3	28 Sep 2010
080	05:35:25.19	-05:05:9.5	1342205226-27	135	0.155	1	A	···	3	···	3	A	OMC 2-3	28 Sep 2010
081	05:35:27.95	-05:04:58.2	1342205226-27	135	1.990	1	A	4.030	1	8.240	1	A	OMC 2-3	28 Sep 2010
082	05:35:19.73	-05:04:54.6	1342205226-27	135	3.780	1	P	7.280	1	10.400	1	A	OMC 2-3	28 Sep 2010
083	05:35:55.73	-05:04:37.6	···	···	···	0	A	···	3	···	0	A	···	···
084	05:35:26.57	-05:03:55.1	1342205226-27	135	104.000	1	A	117.000	1	132.000	1	A	OMC 2-3	28 Sep 2010
085	05:35:28.18	-05:03:40.9	1342205226-27	135	29.000	1	A	36.000	1	48.000	1	P	OMC 2-3	28 Sep 2010
086	05:35:23.65	-05:01:40.3	1342204250-51	019	6.100	1	P	86.500	2	19.300	2	A	OMC 2-3	10 Sep 2010
087	05:35:23.47	-05:01:28.7	1342204250-51	019	63.600	1	P	158.000	1	230.000	1	P	OMC 2-3	10 Sep 2010
088	05:35:22.43	-05:01:14.2	1342204250-51	019	32.800	1	A	69.500	1	81.600	1	P	OMC 2-3	10 Sep 2010

Table 1 continued on next page

Table 1 *(continued)*

HOPS	α_{J2000}	δ_{J2000}	OBSID[a]	Group	70μm	flag[b]	Method[c]	100μm	flag[b]	160μm	flag[b]	Method[c]	Field	Observation Date
	h:m:s	^{o} :$'$:$''$			(mJy)			(mJy)		(mJy)				(UT)
(1)	(2)	(3)	(4)	(5)	(6)	(7)	(8)	(9)	(10)	(11)	(12)	(13)	(14)	(15)
089	05:35:19.96	-05:01:2.6	1342204250-51	019	3.340	1	A	···	3	29.600	2	A	OMC 2-3	10 Sep 2010
090	05:35:34.47	-05:00:52.0	1342204250-51	019	2.370	1	A	1.780	1	0.416	2	A	OMC 2-3	10 Sep 2010
091	05:35:18.91	-05:00:50.9	1342204250-51	019	3.350	1	P	15.800	1	34.300	1	P	OMC 2-3	10 Sep 2010
092	05:35:18.32	-05:00:33.0	1342204250-51	019	33.000	1	A	51.000	1	56.200	1	P	OMC 2-3	10 Sep 2010
093	05:35:15.03	-05:00:8.2	1342204250-51	019	2.490	1	A	···	3	49.000	2	A	OMC 2-3	10 Sep 2010
094	05:35:16.15	-05:00:2.3	1342204250-51	019	6.340	1	A	18.000	1	32.800	1	P	OMC 2-3	10 Sep 2010
095	05:35:34.20	-04:59:52.2	1342204250-51	019	0.632	1	P	2.420	1	5.900	1	P	OMC 2-3	10 Sep 2010
096	05:35:29.72	-04:58:48.8	1342204250-51	019	6.900	1	A	20.100	1	51.200	1	A	OMC 2-3	10 Sep 2010
097	05:35:28.89	-04:57:38.9	1342204250-51	019	···	3	A	···	3	···	3	A	OMC 2-3	10 Sep 2010
098	05:35:19.32	-04:55:44.9	1342204250-51	019	1.650	1	P	···	3	4.640	2	A	OMC 2-3	10 Sep 2010
099	05:34:29.50	-04:55:30.6	1342217754-55	021	3.600	1	A	6.190	1	8.850	1	A	OMC 2-3	31 Mar 2011
100	05:34:21.39	-04:55:14.8	1342217754-55	021	0.015	1	A	···	3	2.330	2	A	OMC 2-3	31 Mar 2011
101	05:35:8.22	-04:54:9.7	1342217758-59	020	2.840	1	A	···	3	48.100	2	A	OMC 2-3	31 Mar 2011
102	05:34:35.18	-04:52:17.9	1342217754-55	021	0.640	1	A	0.693	1	4.680	2	A	OMC 2-3	31 Mar 2011
103	05:34:12.19	-04:50:7.0	1342217754-55	021	···	3	A	···	3	···	3	A	OMC 2-3	31 Mar 2011
104	05:35:6.78	-04:50:1.8	1342217758-59	020	···	3	A	···	3	···	3	A	OMC 2-3	31 Mar 2011
105	05:35:32.28	-04:46:48.5	1342191970-71	306	0.259	1	A	···	3	1.130	2	A	OMC 2-3	10 Mar 2010
106	05:36:12.43	-04:45:15.7	···	···	···	0	A	···	3	···	0	A	···	···
107	05:35:23.34	-04:40:10.5	1342217756-57	024	4.370	1	A	5.060	1	5.560	1	A	OMC 2-3	31 Mar 2011
108	05:35:27.07	-05:10:0.4	1342205228-29	130	40.800	1	P	288.000	2	270.000	1	P	OMC 2-3	28 Sep 2010
109	05:35:8.56	-05:35:59.2	1342205234-35	015	···	0	A	···	0	···	0	A	ONC-S	28 Sep 2010
110	05:36:2.23	-05:02:49.8	···	···	···	0	A	···	3	···	0	A	···	···
111	05:35:23.36	-05:12:2.8	1342205226-27	135	···	0	A	···	0	···	0	A	OMC 2-3	28 Sep 2010

Table 1 continued on next page

Table 1 *(continued)*

HOPS	α_{J2000}	δ_{J2000}	OBSID[a]	Group	70μm	flag[b]	Method[c]	100μm	flag[b]	160μm	flag[b]	Method[c]	Field	Observation Date
	h:m:s	^{o} :$'$:$''$			(mJy)			(mJy)		(mJy)				(UT)
(1)	(2)	(3)	(4)	(5)	(6)	(7)	(8)	(9)	(10)	(11)	(12)	(13)	(14)	(15)
112	05:40:43.99	-07:22:42.9	···	···	···	0	A	···	3	···	0	A	···	···
113	05:39:58.13	-07:26:41.2	1342215589-90	025	0.059	1	A	···	3	0.256	2	A	LDN 1641-C	7 Mar 2011
114	05:40:1.37	-07:25:38.6	1342215589-90	025	0.111	1	A	0.140	1	0.124	2	A	LDN 1641-C	7 Mar 2011
115	05:39:56.50	-07:25:51.5	1342215589-90	025	0.260	1	A	0.287	1	0.258	1	P	LDN 1641-C	7 Mar 2011
116	05:39:57.90	-07:25:13.1	1342215589-90	025	0.328	1	A	0.302	1	0.398	1	P	LDN 1641-C	7 Mar 2011
117	05:39:55.44	-07:24:19.5	1342215589-90	025	0.123	1	A	0.179	1	0.243	1	P	LDN 1641-C	7 Mar 2011
118	05:39:54.58	-07:24:14.8	1342215589-90	025	0.129	1	A	0.073	1	0.078	2	A	LDN 1641-C	7 Mar 2011
119	05:39:50.65	-07:23:30.4	1342215589-90	025	0.746	1	A	0.682	1	0.578	1	P	LDN 1641-C	7 Mar 2011
120	05:39:34.32	-07:26:11.4	1342218729-30	026	0.162	1	A	0.169	1	0.539	1	P	LDN 1641-C	17 Apr 2011
121	05:39:33.70	-07:23:2.0	1342227084-85	313	0.427	1	A	1.260	1	2.880	2	A	LDN 1641-C	22 Aug 2011
122	05:39:45.13	-07:19:13.5	1342215589-90	025	0.045	1	A	···	3	···	3	A	LDN 1641-C	7 Mar 2011
123	05:39:33.30	-07:22:57.4	1342227084-85	313	0.614	1	A	1.260	1	2.470	1	A	LDN 1641-C	22 Aug 2011
124	05:39:19.98	-07:26:11.2	1342218729-30	026	165.000	1	A	233.000	1	236.000	1	A	LDN 1641-C	17 Apr 2011
125	05:39:19.61	-07:26:18.8	1342218729-30	026	21.600	1	P	233.000	2	···	3	A	LDN 1641-C	17 Apr 2011
126	05:40:9.80	-07:09:53.9	···	···	···	0	A	···	3	···	0	A	···	···
127	05:39:0.94	-07:20:22.6	1342227086-87	028	0.754	1	A	0.872	1	1.270	1	A	LDN 1641-C	22 Aug 2011
128	05:38:52.01	-07:21:6.0	1342227086-87	028	0.398	1	P	0.738	1	0.517	1	P	LDN 1641-C	22 Aug 2011
129	05:39:11.85	-07:10:35.0	1342204252-53	029	3.490	1	A	4.920	1	4.270	1	P	LDN 1641-C	10 Sep 2010
130	05:39:2.96	-07:12:52.3	1342204252-53	029	2.170	1	A	2.930	1	2.450	1	A	LDN 1641-C	10 Sep 2010
131	05:39:7.57	-07:10:52.1	1342204252-53	029	0.386	1	A	0.459	1	0.489	1	A	LDN 1641-C	10 Sep 2010
132	05:39:5.36	-07:11:5.2	1342204252-53	029	0.678	1	A	0.562	1	0.667	1	A	LDN 1641-C	10 Sep 2010
133	05:39:5.83	-07:10:39.4	1342204252-53	029	6.980	1	A	8.280	1	9.370	1	A	LDN 1641-C	10 Sep 2010
134	05:38:42.78	-07:12:43.8	1342204254-55	030	3.450	1	A	3.580	1	3.290	1	A	LDN 1641-C	10 Sep 2010

Table 1 continued on next page

Table 1 *(continued)*

HOPS	α_{J2000}	δ_{J2000}	OBSID[a]	Group	70μm	flag[b]	Method[c]	100μm	flag[b]	160μm	flag[b]	Method[c]	Field	Observation Date
	h:m:s	^{o} :$'$:$''$			(mJy)			(mJy)		(mJy)				(UT)
(1)	(2)	(3)	(4)	(5)	(6)	(7)	(8)	(9)	(10)	(11)	(12)	(13)	(14)	(15)
135	05:38:45.31	-07:10:55.9	1342204254-55	030	2.360	1	A	2.490	1	2.530	1	A	LDN 1641-C	10 Sep 2010
136	05:38:46.54	-07:05:37.5	1342205242-43	312	1.670	1	A	2.030	1	2.110	1	P	LDN 1641-C	28 Sep 2010
137	05:38:53.95	-07:02:33.2	1342204256-57	031	0.037	1	A	···	3	0.202	2	A	LDN 1641-C	10 Sep 2010
138	05:38:48.33	-07:02:43.4	1342205242-43	312	0.052	1	A	···	3	1.350	2	A	LDN 1641-C	28 Sep 2010
139	05:38:49.62	-07:01:17.8	1342204256-57	031	6.450	1	A	6.250	1	7.360	1	A	LDN 1641-C	10 Sep 2010
140	05:38:46.28	-07:01:53.5	1342204256-57	031	1.120	1	A	1.450	1	1.940	1	P	LDN 1641-C	10 Sep 2010
141	05:38:48.01	-07:00:49.5	1342204256-57	031	0.104	1	A	···	3	0.307	2	A	LDN 1641-C	10 Sep 2010
142	05:38:47.77	-07:00:26.9	1342204256-57	031	0.074	1	A	···	3	0.985	2	A	LDN 1641-C	10 Sep 2010
143	05:38:46.19	-07:00:48.6	1342204256-57	031	5.390	1	A	6.500	1	6.900	1	A	LDN 1641-C	10 Sep 2010
144	05:38:45.01	-07:01:1.7	1342204256-57	031	4.840	1	P	13.400	2	13.600	2	A	LDN 1641-C	10 Sep 2010
145	05:38:43.84	-07:01:13.2	1342204256-57	031	4.300	1	A	3.940	1	2.700	1	P	LDN 1641-C	10 Sep 2010
146	05:38:44.16	-07:00:40.4	1342204256-57	031	···	3	A	···	3	3.470	2	A	LDN 1641-C	10 Sep 2010
147	05:38:55.00	-06:56:18.6	1342204256-57	031	0.045	1	A	···	3	0.032	2	A	LDN 1641-C	10 Sep 2010
148	05:38:39.51	-06:59:30.3	1342204256-57	031	0.553	1	A	0.466	1	0.419	1	P	LDN 1641-C	10 Sep 2010
149	05:38:40.48	-06:58:21.7	1342204256-57	031	7.770	1	A	7.550	1	5.880	1	A	LDN 1641-C	10 Sep 2010
150	05:38:7.53	-07:08:29.2	1342227045-46	032	6.180	1	A	7.410	1	9.580	1	A	LDN 1641-C	21 Aug 2011
151	05:38:42.88	-06:56:40.7	1342204256-57	031	···	3	A	···	3	···	3	A	LDN 1641-C	10 Sep 2010
152	05:37:58.76	-07:07:25.3	1342227045-46	032	1.330	1	A	1.860	1	3.140	1	P	LDN 1641-C	21 Aug 2011
153	05:37:57.01	-07:06:56.5	1342227045-46	032	7.250	1	A	17.000	1	29.600	1	A	LDN 1641-C	21 Aug 2011
154	05:38:20.09	-06:59:4.8	1342228171-72	033	0.167	1	A	0.150	1	0.163	1	A	LDN 1641-C	4 Sep 2011
155	05:37:15.84	-07:17:50.0	···	···	···	0	A	···	3	···	0	A	···	···
156	05:38:3.40	-06:58:15.8	1342205240-41	034	0.673	1	A	0.773	1	1.050	1	P	LDN 1641-C	28 Sep 2010
157	05:37:56.57	-06:56:39.2	1342205240-41	034	7.620	1	A	11.400	1	11.100	1	A	LDN 1641-C	28 Sep 2010

Table 1 continued on next page

Table 1 *(continued)*

HOPS	α_{J2000}	δ_{J2000}	OBSID[a]	Group	70μm	flag[b]	Method[c]	100μm	flag[b]	160μm	flag[b]	Method[c]	Field	Observation Date
	h:m:s	^{o} :$'$:$''$			(mJy)			(mJy)		(mJy)				(UT)
(1)	(2)	(3)	(4)	(5)	(6)	(7)	(8)	(9)	(10)	(11)	(12)	(13)	(14)	(15)
158	05:37:24.46	-06:58:32.8	1342227314-15	035	1.450	1	A	1.400	1	1.480	1	P	LDN 1641-C	24 Aug 2011
159	05:37:53.74	-06:47:16.9	1342227088-89	036	0.227	1	A	0.216	1	0.161	1	A	LDN 1641-N	22 Aug 2011
160	05:37:51.04	-06:47:20.4	1342227088-89	036	2.850	1	A	4.110	1	3.860	1	P	LDN 1641-N	22 Aug 2011
161	05:36:34.76	-07:11:13.7	···	···	···	0	A	0.231	1	···	0	A	···	···
162	05:36:30.97	-06:52:40.9	···	···	···	0	A	···	3	···	0	A	···	···
163	05:37:17.28	-06:36:18.2	1342227090-91	037	0.878	1	A	0.721	1	0.765	1	A	LDN 1641-N	22 Aug 2011
164	05:37:0.45	-06:37:10.5	1342227090-91	037	0.738	1	A	1.720	1	4.100	1	A	LDN 1641-N	22 Aug 2011
165	05:36:23.54	-06:46:14.6	1342205238-39	038	2.560	1	P	···	3	73.400	2	A	LDN 1641-N	28 Sep 2010
166	05:36:25.13	-06:44:41.8	1342205238-39	038	17.800	1	A	18.600	1	15.800	1	A	LDN 1641-N	28 Sep 2010
167	05:36:19.79	-06:46:0.9	1342205238-39	038	0.203	1	A	···	3	4.010	2	A	LDN 1641-N	28 Sep 2010
168	05:36:18.93	-06:45:22.7	1342205238-39	038	147.000	1	A	182.000	1	124.000	1	A	LDN 1641-N	28 Sep 2010
169	05:36:36.12	-06:38:51.9	1342227094-95	040	5.090	1	A	15.800	1	28.800	1	A	LDN 1641-N	22 Aug 2011
170	05:36:41.33	-06:34:0.1	1342227092-93	039	1.150	1	A	1.030	1	0.905	1	A	LDN 1641-N	22 Aug 2011
171	05:36:17.20	-06:38:1.6	1342227094-95	040	4.440	1	A	6.250	1	6.200	1	P	LDN 1641-N	22 Aug 2011
172	05:36:19.44	-06:29:6.8	1342227316-17	041	1.040	1	P	1.250	1	1.980	1	P	LDN 1641-N	24 Aug 2011
173	05:36:26.04	-06:25:5.2	1342205236-37	042	2.150	1	P	4.580	1	5.260	1	P	LDN 1641-N	28 Sep 2010
174	05:36:25.86	-06:24:58.7	1342205236-37	042	1.620	1	P	4.580	2	7.930	2	A	LDN 1641-N	28 Sep 2010
175	05:36:24.06	-06:24:54.9	1342205236-37	042	0.286	1	A	4.160	2	8.800	2	A	LDN 1641-N	28 Sep 2010
176	05:36:23.58	-06:24:51.6	1342205236-37	042	0.947	1	P	4.160	2	5.730	1	P	LDN 1641-N	28 Sep 2010
177	05:35:50.02	-06:34:53.4	1342227310-11	043	1.090	1	A	1.330	1	1.170	1	P	LDN 1641-N	24 Aug 2011
178	05:36:24.61	-06:22:41.3	1342205236-37	042	36.500	1	A	42.000	1	40.200	1	A	LDN 1641-N	28 Sep 2010
179	05:36:21.84	-06:23:29.8	1342205236-37	042	1.790	1	A	2.550	1	3.870	1	P	LDN 1641-N	28 Sep 2010
180	05:36:59.39	-06:10:15.6	···	···	···	0	A	···	3	···	0	A	···	···

Table 1 continued on next page

Table 1 *(continued)*

HOPS	α_{J2000}	δ_{J2000}	OBSID[a]	Group	70μm	flag[b]	Method[c]	100μm	flag[b]	160μm	flag[b]	Method[c]	Field	Observation Date
	h:m:s	^{o} :$'$:$''$			(mJy)			(mJy)		(mJy)				(UT)
(1)	(2)	(3)	(4)	(5)	(6)	(7)	(8)	(9)	(10)	(11)	(12)	(13)	(14)	(15)
181	05:36:19.50	-06:22:12.4	1342205236-37	042	11.300	1	P	286.000	2	···	3	A	LDN 1641-N	28 Sep 2010
182	05:36:18.83	-06:22:10.2	1342205236-37	042	174.000	1	A	286.000	1	265.000	1	A	LDN 1641-N	28 Sep 2010
183	05:36:17.86	-06:22:28.1	1342205236-37	042	0.959	1	P	···	3	···	3	A	LDN 1641-N	28 Sep 2010
184	05:36:12.95	-06:23:30.6	1342205236-37	042	0.282	1	A	0.500	1	0.661	1	A	LDN 1641-N	28 Sep 2010
185	05:36:36.98	-06:14:58.0	1342204258-59	044	1.610	1	A	2.820	1	6.830	1	P	LDN 1641-N	10 Sep 2010
186	05:35:47.28	-06:26:14.7	1342215593-94	045	1.400	1	A	1.590	1	2.220	1	A	LDN 1641-N	7 Mar 2011
187	05:35:50.94	-06:22:43.5	1342215593-94	045	0.053	1	A	···	3	···	3	A	LDN 1641-N	7 Mar 2011
188	05:35:29.82	-06:26:58.2	1342215593-94	045	39.600	1	A	37.600	1	34.300	1	A	LDN 1641-N	7 Mar 2011
189	05:35:30.89	-06:26:32.1	1342215593-94	045	1.630	1	A	3.620	1	4.850	1	P	LDN 1641-N	7 Mar 2011
190	05:35:28.50	-06:27:1.8	1342215593-94	045	0.201	1	P	···	3	5.880	2	A	LDN 1641-N	7 Mar 2011
191	05:36:17.26	-06:11:11.0	1342227324-25	047	1.010	1	A	1.070	1	1.570	1	P	LDN 1641-N	24 Aug 2011
192	05:36:32.45	-06:01:16.2	1342217444-45	048	2.150	1	A	3.230	1	3.740	1	P	ONC-S	30 Mar 2011
193	05:36:30.27	-06:01:17.4	1342217444-45	048	1.460	1	A	1.610	1	1.710	1	P	ONC-S	30 Mar 2011
194	05:35:52.00	-06:10:1.8	1342227322-23	049	10.400	1	A	10.500	1	12.300	1	A	LDN 1641-N	24 Aug 2011
195	05:36:0.06	-06:07:14.2	1342227322-23	049	···	3	A	···	3	···	3	A	LDN 1641-N	24 Aug 2011
196	05:35:20.91	-06:18:22.3	···	···	···	0	A	0.180	1	···	0	A	···	···
197	05:34:15.88	-06:34:32.7	1342217748-49	050	0.198	1	A	0.189	1	0.065	1	A	LDN 1641-N	31 Mar 2011
198	05:35:22.18	-06:13:6.2	1342227318-19	051	2.280	1	A	3.570	1	4.230	1	P	LDN 1641-N	24 Aug 2011
199	05:34:39.86	-06:25:14.2	1342203649-50	311	0.114	1	A	0.117	1	0.183	1	P	LDN 1641-N	26 Aug 2010
200	05:35:33.21	-06:06:9.6	1342227320-21	052	0.443	1	A	0.437	1	0.450	1	A	LDN 1641-N	24 Aug 2011
201	05:34:6.94	-06:32:8.0	1342217748-49	050	0.070	1	A	···	3	0.701	2	A	LDN 1641-N	31 Mar 2011
202	05:33:43.92	-06:13:46.2	···	···	···	0	A	···	3	···	0	A	···	···
203	05:36:22.84	-06:46:6.2	1342205238-39	038	45.100	1	A	80.700	1	105.000	1	A	LDN 1641-N	28 Sep 2010

Table 1 continued on next page

Table 1 *(continued)*

HOPS	α_{J2000}	δ_{J2000}	OBSID[a]	Group	70μm	flag[b]	Method[c]	100μm	flag[b]	160μm	flag[b]	Method[c]	Field	Observation Date
	h:m:s	^{o} :$'$:$''$			(mJy)			(mJy)		(mJy)				(UT)
(1)	(2)	(3)	(4)	(5)	(6)	(7)	(8)	(9)	(10)	(11)	(12)	(13)	(14)	(15)
204	05:43:10.18	-08:46:7.9	1342218735-36	053	3.410	1	A	4.500	1	6.200	1	A	LDN 1641-S	17 Apr 2011
205	05:43:2.88	-08:47:49.4	1342218735-36	053	0.062	1	A	···	3	0.753	2	A	LDN 1641-S	17 Apr 2011
206	05:43:7.26	-08:44:31.1	1342218735-36	053	5.510	1	P	6.330	1	9.080	1	P	LDN 1641-S	17 Apr 2011
207	05:42:38.58	-08:50:18.6	1342218796-97	054	0.346	1	A	0.465	1	0.679	1	A	LDN 1641-S	18 Apr 2011
208	05:42:52.72	-08:44:12.7	1342218735-36	053	0.008	1	A	···	3	0.431	2	A	LDN 1641-S	17 Apr 2011
209	05:42:52.89	-08:41:41.2	1342218798-99	055	0.276	1	A	0.191	1	0.224	1	A	LDN 1641-S	18 Apr 2011
210	05:42:58.27	-08:38:5.4	1342205256-57	056	2.170	1	A	2.530	1	2.110	1	P	LDN 1641-S	28 Sep 2010
211	05:42:58.36	-08:37:43.5	1342218798-99	055	0.545	1	A	1.340	1	1.100	1	P	LDN 1641-S	18 Apr 2011
212	05:42:58.39	-08:37:41.6	1342205256-57	056	···	0	A	···	0	···	0	A	LDN 1641-S	28 Sep 2010
213	05:42:48.09	-08:40:8.3	1342218798-99	055	1.080	1	A	1.020	1	1.090	1	A	LDN 1641-S	18 Apr 2011
214	05:42:47.22	-08:36:36.6	1342205256-57	056	0.131	1	A	0.165	1	0.095	1	A	LDN 1641-S	28 Sep 2010
215	05:43:9.58	-08:29:27.1	1342218788-89	058	1.020	1	A	0.864	1	0.982	1	A	LDN 1641-S	18 Apr 2011
216	05:42:55.54	-08:32:48.3	1342218794-95	059	1.410	1	A	1.370	1	1.300	1	P	LDN 1641-S	18 Apr 2011
217	05:43:11.16	-08:24:20.1	···	···	···	0	A	···	3	···	0	A	···	···
218	05:43:9.90	-08:13:23.5	···	···	···	0	A	···	3	···	0	A	···	···
219	05:41:29.25	-08:43:4.3	1342215359-60	060	4.740	1	A	4.880	1	4.330	1	A	LDN 1641-S	6 Mar 2011
220	05:41:29.78	-08:42:46.0	1342215359-60	060	0.407	1	P	0.471	1	0.456	1	A	LDN 1641-S	6 Mar 2011
221	05:42:47.05	-08:17:7.0	1342205254-55	061	14.900	1	A	16.800	1	15.600	1	A	LDN 1641-S	28 Sep 2010
222	05:41:26.68	-08:42:24.5	1342215359-60	060	0.420	1	A	0.474	1	0.257	1	P	LDN 1641-S	6 Mar 2011
223	05:42:48.46	-08:16:34.5	1342205254-55	061	16.100	1	A	19.500	1	20.700	1	A	LDN 1641-S	28 Sep 2010
224	05:41:32.03	-08:40:9.7	1342215359-60	060	6.810	1	A	11.800	1	14.500	1	A	LDN 1641-S	6 Mar 2011
225	05:41:30.35	-08:40:17.6	1342215359-60	060	0.652	1	P	1.240	2	0.784	1	A	LDN 1641-S	6 Mar 2011
226	05:41:30.06	-08:40:9.4	1342215359-60	060	1.060	1	P	1.300	1	0.997	1	P	LDN 1641-S	6 Mar 2011

Table 1 continued on next page

Table 1 *(continued)*

HOPS	α_{J2000}	δ_{J2000}	OBSID[a]	Group	70μm	flag[b]	Method[c]	100μm	flag[b]	160μm	flag[b]	Method[c]	Field	Observation Date
	h:m:s	^{o} :$'$:$''$			(mJy)			(mJy)		(mJy)				(UT)
(1)	(2)	(3)	(4)	(5)	(6)	(7)	(8)	(9)	(10)	(11)	(12)	(13)	(14)	(15)
227	05:41:32.33	-08:37:55.5	1342218790-91	117	0.429	1	A	0.351	1	0.416	1	A	LDN 1641-S	18 Apr 2011
228	05:41:34.17	-08:35:27.7	1342218790-91	117	14.100	1	A	14.600	1	13.700	1	A	LDN 1641-S	18 Apr 2011
229	05:42:47.37	-08:10:8.8	1342218792-93	062	0.128	1	A	0.174	1	0.302	1	P	LDN 1641-S	18 Apr 2011
230	05:42:30.80	-08:09:5.3	···	···	···	0	A	···	3	···	0	A	···	···
231	05:40:28.54	-08:32:55.1	···	···	···	0	A	···	3	···	0	A	···	···
232	05:41:35.45	-08:08:22.5	1342218800-01	063	1.090	1	A	0.727	1	0.742	1	P	LDN 1641-S	18 Apr 2011
233	05:41:52.31	-08:01:22.0	1342205252-53	064	0.122	1	A	0.170	1	0.702	2	A	LDN 1641-S	28 Sep 2010
234	05:41:49.95	-08:01:26.5	1342205252-53	064	4.860	1	A	5.720	1	5.220	1	P	LDN 1641-S	28 Sep 2010
235	05:41:25.34	-08:05:54.8	1342205250-51	118	2.470	1	A	2.260	1	1.910	1	A	LDN 1641-S	28 Sep 2010
236	05:41:30.21	-08:03:41.5	1342205250-51	118	6.510	1	A	7.080	1	6.050	1	A	LDN 1641-S	28 Sep 2010
237	05:41:28.97	-08:03:25.8	1342205250-51	118	0.450	1	P	0.494	1	0.586	1	P	LDN 1641-S	28 Sep 2010
238	05:41:26.64	-08:03:12.6	1342205250-51	118	0.451	1	A	0.429	1	0.307	1	P	LDN 1641-S	28 Sep 2010
239	05:41:27.06	-08:00:54.8	1342215591-92	065	0.330	1	A	0.628	1	0.673	2	A	LDN 1641-S	7 Mar 2011
240	05:41:25.97	-08:01:15.9	1342215591-92	065	0.174	1	A	···	3	0.232	2	A	LDN 1641-S	7 Mar 2011
241	05:41:26.40	-08:01:2.1	1342215591-92	065	1.460	1	P	1.690	1	1.750	1	P	LDN 1641-S	7 Mar 2011
242	05:40:48.52	-08:11:9.0	1342206322-23	119	0.181	1	A	0.119	1	0.109	1	A	LDN 1641-S	11 Oct 2010
243	05:41:1.66	-08:06:44.8	1342215361-62	066	0.953	1	A	1.140	1	1.780	1	P	LDN 1641-S	6 Mar 2011
244	05:41:1.99	-08:06:1.9	1342215361-62	066	3.320	1	A	4.010	1	4.420	1	A	LDN 1641-S	6 Mar 2011
245	05:41:22.86	-07:58:56.0	1342215591-92	065	0.266	1	A	0.239	1	0.202	1	P	LDN 1641-S	7 Mar 2011
246	05:40:47.12	-08:09:47.8	1342206322-23	119	0.817	1	A	0.846	1	1.120	1	A	LDN 1641-S	11 Oct 2010
247	05:41:26.22	-07:56:51.6	1342205248-49	121	4.740	1	A	13.000	1	18.400	1	A	LDN 1641-S	28 Sep 2010
248	05:41:22.09	-07:58:3.0	1342215591-92	065	1.360	1	A	1.010	1	0.719	1	P	LDN 1641-S	7 Mar 2011
249	05:40:52.86	-08:05:48.8	1342215361-62	066	0.056	1	A	0.074	1	1.010	2	A	LDN 1641-S	6 Mar 2011

Table 1 continued on next page

Table 1 *(continued)*

HOPS	α_{J2000}	δ_{J2000}	OBSID[a]	Group	70μm	flag[b]	Method[c]	100μm	flag[b]	160μm	flag[b]	Method[c]	Field	Observation Date
	h:m:s	^{o} :$'$:$''$			(mJy)			(mJy)		(mJy)				(UT)
(1)	(2)	(3)	(4)	(5)	(6)	(7)	(8)	(9)	(10)	(11)	(12)	(13)	(14)	(15)
250	05:40:48.84	-08:06:57.2	1342215361-62	066	17.300	1	A	19.500	1	16.600	1	A	LDN 1641-S	6 Mar 2011
251	05:40:54.01	-08:05:13.0	1342215361-62	066	0.655	1	A	0.698	1	0.825	1	P	LDN 1641-S	6 Mar 2011
252	05:40:49.92	-08:06:8.3	1342215361-62	066	3.040	1	A	3.220	1	4.000	1	P	LDN 1641-S	6 Mar 2011
253	05:41:28.77	-07:53:51.0	1342205248-49	121	0.877	1	A	1.080	1	1.240	1	A	LDN 1641-S	28 Sep 2010
254	05:41:24.52	-07:55:7.3	1342205248-49	121	11.300	1	A	12.600	1	13.400	1	A	LDN 1641-S	28 Sep 2010
255	05:40:50.57	-08:05:48.7	1342215361-62	066	0.292	1	A	0.340	1	1.410	2	A	LDN 1641-S	6 Mar 2011
256	05:40:45.26	-08:06:42.2	1342215361-62	066	0.169	1	A	0.363	1	1.840	2	A	LDN 1641-S	6 Mar 2011
257	05:41:19.87	-07:55:46.6	1342205248-49	121	0.436	1	A	0.735	1	0.827	1	P	LDN 1641-S	28 Sep 2010
258	05:41:24.71	-07:54:8.5	1342205248-49	121	0.907	1	A	1.430	1	2.110	1	P	LDN 1641-S	28 Sep 2010
259	05:40:20.88	-08:13:55.2	1342227078-79	067	0.714	1	A	0.896	1	0.828	1	P	LDN 1641-S	22 Aug 2011
260	05:40:19.39	-08:14:16.4	1342227078-79	067	1.540	1	A	1.690	1	2.070	1	A	LDN 1641-S	22 Aug 2011
261	05:41:18.89	-07:55:29.1	1342205248-49	121	4.660	1	A	5.510	1	7.050	1	A	LDN 1641-S	28 Sep 2010
262	05:41:23.97	-07:53:42.0	1342205248-49	121	1.120	1	P	3.130	2	2.470	1	P	LDN 1641-S	28 Sep 2010
263	05:41:23.68	-07:53:46.8	1342205248-49	121	1.140	1	P	3.130	2	3.490	1	P	LDN 1641-S	28 Sep 2010
264	05:40:59.11	-08:00:14.3	1342215361-62	066	0.056	1	A	···	3	0.041	2	A	LDN 1641-S	6 Mar 2011
265	05:41:20.32	-07:53:10.6	1342205248-49	121	0.070	1	A	···	3	1.920	2	A	LDN 1641-S	28 Sep 2010
266	05:41:11.81	-07:53:35.8	1342205248-49	121	0.061	1	A	0.076	1	0.101	1	A	LDN 1641-S	28 Sep 2010
267	05:41:19.66	-07:50:41.0	1342227848-49	068	1.500	1	A	1.440	1	1.320	1	A	LDN 1641-S	3 Sep 2011
268	05:40:38.33	-08:00:36.0	1342227080-81	069	2.790	1	A	2.620	1	2.420	1	A	LDN 1641-S	22 Aug 2011
269	05:41:27.01	-07:42:33.8	···	···	···	0	A	0.065	1	···	0	A	···	···
270	05:40:40.53	-07:54:39.8	1342228167-68	070	0.622	1	A	0.614	1	0.698	1	P	LDN 1641-S	4 Sep 2011
271	05:40:43.96	-07:49:30.4	1342228163-64	071	0.127	1	A	0.157	1	0.230	1	P	LDN 1641-S	4 Sep 2011
272	05:40:20.53	-07:56:39.6	1342218733-34	072	2.470	1	P	3.670	1	3.470	1	P	LDN 1641-S	17 Apr 2011

Table 1 continued on next page

Table 1 *(continued)*

HOPS	α_{J2000}	δ_{J2000}	OBSID[a]	Group	70μm	flag[b]	Method[c]	100μm	flag[b]	160μm	flag[b]	Method[c]	Field	Observation Date
	h:m:s	^{o} :$'$:$''$			(mJy)			(mJy)		(mJy)				(UT)
(1)	(2)	(3)	(4)	(5)	(6)	(7)	(8)	(9)	(10)	(11)	(12)	(13)	(14)	(15)
273	05:40:20.88	-07:56:24.7	1342218733-34	072	2.520	1	P	3.300	1	3.080	1	P	LDN 1641-S	17 Apr 2011
274	05:40:20.71	-07:54:59.7	1342218733-34	072	1.360	1	A	1.230	1	1.460	1	A	LDN 1641-S	17 Apr 2011
275	05:40:36.35	-07:49:7.0	1342228163-64	071	0.162	1	A	0.173	1	0.097	1	A	LDN 1641-S	4 Sep 2011
276	05:40:42.91	-07:45:1.9	1342228325-26	073	0.124	1	A	0.072	1	0.067	2	A	LDN 1641-S	7 Sep 2011
277	05:40:44.36	-07:44:16.7	1342228325-26	073	0.042	1	A	···	3	0.401	2	A	LDN 1641-S	7 Sep 2011
278	05:40:20.35	-07:51:14.9	1342218731-32	074	0.392	1	A	0.335	1	0.602	1	A	LDN 1641-S	17 Apr 2011
279	05:40:17.79	-07:48:26.0	1342218731-32	074	3.900	1	A	3.350	1	2.860	1	A	LDN 1641-S	17 Apr 2011
280	05:40:14.93	-07:48:48.7	1342218731-32	074	6.810	1	A	6.520	1	6.040	1	A	LDN 1641-S	17 Apr 2011
281	05:40:24.62	-07:43:8.3	1342227082-83	075	2.620	1	A	3.230	1	3.620	1	A	LDN 1641-S	22 Aug 2011
282	05:40:26.09	-07:37:32.0	1342205246-47	076	1.920	1	A	2.130	1	1.580	1	A	LDN 1641-S	28 Sep 2010
283	05:40:44.67	-07:29:54.5	1342228327-28	077	0.414	1	A	···	3	0.309	1	A	LDN 1641-C	7 Sep 2011
284	05:38:51.48	-08:01:27.4	1342228169-70	078	0.312	1	A	0.275	1	0.239	1	A	LDN 1641-S	4 Sep 2011
285	05:40:5.90	-07:29:32.9	1342205244-45	079	0.335	1	A	0.428	1	0.483	1	A	LDN 1641-C	28 Sep 2010
286	05:39:58.70	-07:31:12.1	1342205244-45	079	1.350	1	A	1.710	1	1.410	1	P	LDN 1641-C	28 Sep 2010
287	05:40:8.78	-07:27:27.7	1342228161-62	123	1.500	1	A	1.760	1	2.310	1	A	LDN 1641-C	4 Sep 2011
288	05:39:55.94	-07:30:28.0	1342205244-45	079	454.000	1	A	468.000	1	427.000	1	P	LDN 1641-C	28 Sep 2010
289	05:39:56.75	-07:30:6.1	1342215589-90	025	···	3	A	···	3	···	3	A	LDN 1641-C	7 Mar 2011
290	05:39:57.41	-07:29:33.4	1342205244-45	079	3.020	1	A	6.460	1	9.970	1	A	LDN 1641-C	28 Sep 2010
291	05:39:57.97	-07:28:57.5	1342205244-45	079	0.119	1	A	0.165	1	7.060	2	A	LDN 1641-C	28 Sep 2010
292	05:37:54.88	-07:41:20.3	···	···	···	0	A	0.282	1	···	0	A	···	···
293	05:40:58.89	-07:48:2.1	1342228165-66	320	0.037	1	A	···	3	0.057	2	A	LDN 1641-S	4 Sep 2011
294	05:40:51.72	-02:26:48.6	1342226729-30	080	1.810	1	P	3.040	1	3.070	1	P	NGC 2023-4	18 Aug 2011
295	05:41:28.94	-02:23:19.4	1342226733-34	081	0.656	1	P	1.070	1	1.230	1	P	NGC 2023-4	18 Aug 2011

Table 1 continued on next page

Table 1 *(continued)*

HOPS	α_{J2000}	δ_{J2000}	OBSID[a]	Group	70μm	flag[b]	Method[c]	100μm	flag[b]	160μm	flag[b]	Method[c]	Field	Observation Date
	h:m:s	^{o} :$'$:$''$			(mJy)			(mJy)		(mJy)				(UT)
(1)	(2)	(3)	(4)	(5)	(6)	(7)	(8)	(9)	(10)	(11)	(12)	(13)	(14)	(15)
296	05:41:17.17	-02:18:7.6	1342227049-50	083	···	3	A	···	3	···	3	A	NGC 2023-4	21 Aug 2011
297	05:41:23.27	-02:17:35.8	1342228913-14	082	0.196	1	P	···	3	8.700	2	A	NGC 2023-4	19 Sep 2011
298	05:41:37.17	-02:17:17.0	1342227049-50	083	35.700	1	A	29.100	1	21.500	1	P	NGC 2023-4	21 Aug 2011
299	05:41:44.58	-02:16:6.3	1342227049-50	083	12.800	1	P	20.300	2	11.800	1	P	NGC 2023-4	21 Aug 2011
300	05:41:24.21	-02:16:6.4	1342228913-14	082	1.410	1	P	4.150	2	3.260	1	P	NGC 2023-4	19 Sep 2011
301	05:41:44.77	-02:15:55.3	1342227049-50	083	3.070	1	P	···	3	22.400	2	A	NGC 2023-4	21 Aug 2011
302	05:40:22.41	-02:15:39.7	···	···	···	0	A	···	3	···	0	A	···	···
303	05:42:2.62	-02:07:45.7	1342226735-36	085	1.910	1	A	4.140	1	10.700	1	A	NGC 2023-4	18 Aug 2011
304	05:41:45.94	-01:56:26.1	1342227047-48	086	7.530	1	A	···	3	257.000	2	A	NGC 2023-4	21 Aug 2011
305	05:41:45.38	-01:51:56.8	1342227047-48	086	4.090	1	A	···	3	···	3	A	NGC 2023-4	21 Aug 2011
306	05:43:3.12	-01:48:4.6	···	···	···	0	A	···	3	···	0	A	···	···
307	05:41:13.85	-01:47:3.9	···	···	···	0	A	···	3	···	0	A	···	···
308	05:43:13.98	-01:43:10.2	···	···	···	0	A	0.126	1	···	0	A	···	···
309	05:42:47.36	-01:24:47.0	···	···	···	0	A	0.193	1	···	0	A	···	···
310	05:42:27.68	-01:20:1.0	1342205220-21	089	36.700	1	A	49.300	1	50.200	1	A	NGC 2023-4	28 Sep 2010
311	05:43:3.04	-01:16:28.9	1342228376-77	090	3.320	1	A	3.380	1	3.310	1	A	NGC 2023-4	9 Sep 2011
312	05:43:5.70	-01:15:54.3	1342228376-77	090	1.570	1	A	2.780	1	3.940	1	A	NGC 2023-4	9 Sep 2011
313	05:41:0.76	-01:09:10.6	···	···	···	0	A	0.096	1	···	0	A	···	···
314	05:46:36.12	00:20:29.2	···	···	···	0	A	···	3	···	0	A	···	···
315	05:46:3.63	00:14:49.2	1342205218-19	091	9.530	1	A	13.700	1	15.100	1	A	NGC 2068	28 Sep 2010
316	05:46:7.29	00:13:23.0	1342205218-19	091	5.730	1	P	···	3	22.200	1	P	NGC 2068	28 Sep 2010
317	05:46:8.59	00:10:38.5	1342205218-19	091	6.050	1	A	16.400	1	31.500	1	P	NGC 2068	28 Sep 2010
318	05:46:13.50	00:08:55.3	1342205218-19	091	0.153	1	A	0.165	1	2.380	2	A	NGC 2068	28 Sep 2010

Table 1 continued on next page

Table 1 *(continued)*

HOPS	α_{J2000}	δ_{J2000}	OBSID[a]	Group	70μm	flag[b]	Method[c]	100μm	flag[b]	160μm	flag[b]	Method[c]	Field	Observation Date
	h:m:s	^{o} :$'$:$''$			(mJy)			(mJy)		(mJy)				(UT)
(1)	(2)	(3)	(4)	(5)	(6)	(7)	(8)	(9)	(10)	(11)	(12)	(13)	(14)	(15)
319	05:46:13.00	00:08:14.9	1342205218-19	091	0.027	1	A	···	3	2.930	2	A	NGC 2068	28 Sep 2010
320	05:46:14.21	00:05:26.8	1342205216-17	092	0.844	1	P	1.700	1	2.500	1	P	NGC 2068	28 Sep 2010
321	05:46:33.17	00:00:2.2	1342215363-64	093	8.870	1	A	10.700	1	12.700	1	A	NGC 2068	6 Mar 2011
322	05:46:46.49	00:00:16.1	1342215363-64	093	0.816	1	P	4.390	2	32.500	2	A	NGC 2068	6 Mar 2011
323	05:46:47.69	00:00:25.3	1342215363-64	093	15.800	1	P	35.000	1	40.800	1	P	NGC 2068	6 Mar 2011
324	05:46:37.54	00:00:34.0	1342215363-64	093	3.480	1	A	4.820	1	10.700	1	P	NGC 2068	6 Mar 2011
325	05:46:39.25	00:01:15.0	1342215363-64	093	11.200	1	A	25.800	1	32.500	1	A	NGC 2068	6 Mar 2011
326	05:46:39.58	00:04:16.6	1342228365-66	094	0.805	1	P	···	3	4.200	1	P	NGC 2068	9 Sep 2011
327	05:46:27.34	00:08:51.7	···	···	···	0	A	···	3	···	0	A	···	···
328	05:46:13.46	00:10:33.2	···	···	···	0	A	···	3	···	0	A	···	···
329	05:47:1.61	00:17:58.9	1342215587-88	096	6.030	1	P	7.820	1	8.810	1	P	NGC 2068	7 Mar 2011
330	05:46:51.37	00:19:47.4	1342218727-28	128	···	3	A	···	3	···	3	A	NGC 2068	17 Apr 2011
331	05:46:28.32	00:19:49.4	1342228374-75	302	0.880	1	A	1.380	1	1.910	1	P	NGC 2068	9 Sep 2011
332	05:47:31.70	00:20:20.8	1342227966-67	303	···	3	A	10.700	2	···	3	A	NGC 2068	3 Sep 2011
333	05:47:22.88	00:20:58.3	1342227966-67	303	0.210	1	P	0.538	1	0.788	1	A	NGC 2068	3 Sep 2011
334	05:46:48.53	00:21:28.2	1342218727-28	128	0.051	1	A	···	3	1.860	2	A	NGC 2068	17 Apr 2011
335	05:47:5.86	00:22:38.9	1342215587-88	096	0.682	1	P	···	3	2.780	1	P	NGC 2068	7 Mar 2011
336	05:46:2.28	00:23:30.7	1342216450-51	301	0.047	1	A	···	3	0.089	1	A	NGC 2068	20 Mar 2011
337	05:46:55.10	00:23:34.6	1342218727-28	128	1.830	1	A	1.680	1	2.040	1	P	NGC 2068	17 Apr 2011
338	05:46:57.34	00:23:50.2	1342218727-28	128	0.286	1	P	1.300	1	1.730	1	P	NGC 2068	17 Apr 2011
339	05:45:53.59	00:25:27.3	1342216450-51	301	0.104	1	A	0.172	1	0.053	1	A	NGC 2068	20 Mar 2011
340	05:47:1.29	00:26:21.5	1342218727-28	128	3.120	1	P	15.100	2	10.200	1	P	NGC 2068	17 Apr 2011
341	05:47:0.99	00:26:22.2	1342218727-28	128	2.920	1	P	15.100	2	10.200	1	A	NGC 2068	17 Apr 2011

Table 1 continued on next page

Table 1 *(continued)*

HOPS	α_{J2000}	δ_{J2000}	OBSID[a]	Group	70μm	flag[b]	Method[c]	100μm	flag[b]	160μm	flag[b]	Method[c]	Field	Observation Date
	h:m:s	^{o} :$'$:$''$			(mJy)			(mJy)		(mJy)				(UT)
(1)	(2)	(3)	(4)	(5)	(6)	(7)	(8)	(9)	(10)	(11)	(12)	(13)	(14)	(15)
342	05:47:57.09	00:35:27.4	1342227969-70	097	0.287	1	A	0.339	1	0.717	2	A	NGC 2068	3 Sep 2011
343	05:47:59.03	00:35:32.9	1342227969-70	097	9.660	1	A	8.940	1	10.100	1	A	NGC 2068	3 Sep 2011
344	05:47:24.72	00:37:35.2	1342227971-72	098	0.086	1	A	0.109	1	0.055	1	A	NGC 2068	3 Sep 2011
345	05:47:38.98	00:38:36.3	1342227971-72	098	0.646	1	A	0.625	1	1.040	1	A	NGC 2068	3 Sep 2011
346	05:47:42.99	00:40:57.5	1342205214-15	300	0.080	1	A	0.071	1	0.219	1	A	NGC 2068	28 Sep 2010
347	05:47:15.89	00:21:23.8	1342215587-88	096	0.569	1	A	1.630	1	4.840	1	A	NGC 2068	7 Mar 2011
348	05:47:0.27	00:20:37.5	1342215587-88	096	0.682	1	A	···	3	1.120	1	A	NGC 2068	7 Mar 2011
349	05:35:26.20	-05:08:33.4	1342205228-29	130	···	3	A	···	3	···	3	A	OMC 2-3	28 Sep 2010
350	05:35:30.20	-05:08:18.9	1342205228-29	130	2.400	1	A	···	3	23.800	2	A	OMC 2-3	28 Sep 2010
351	05:35:31.42	-05:04:47.1	1342205228-29	130	···	3	A	···	3	···	3	A	OMC 2-3	28 Sep 2010
352	05:35:26.81	-05:04:3.0	1342204250-51	019	···	3	A	···	3	···	3	A	OMC 2-3	10 Sep 2010
353	05:54:13.34	01:43:3.1	1342215365-66	000	···	3	A	···	3	···	3	A	LDN 1622	6 Mar 2011
354	05:54:24.25	01:44:19.4	1342215365-66	000	8.430	1	A	37.100	1	37.900	1	A	LDN 1622	6 Mar 2011
355	05:37:17.08	-06:49:49.3	1342227312-13	101	2.760	1	A	5.780	1	9.790	1	A	LDN 1641-N	24 Aug 2011
356	05:42:8.18	-01:26:37.5	···	···	···	0	A	···	3	···	0	A	···	···
357	05:41:39.10	-01:52:7.5	1342227047-48	086	6.280	1	A	2.900	1	30.200	2	A	NGC 2023-4	21 Aug 2011
358	05:46:7.23	00:13:29.9	1342205218-19	091	62.200	1	A	104.000	1	122.000	1	A	NGC 2068	28 Sep 2010
359	05:47:24.81	00:20:59.9	1342227966-67	303	20.000	1	A	43.600	1	56.100	1	A	NGC 2068	3 Sep 2011
360	05:47:27.09	00:20:33.1	1342227966-67	303	···	3	A	6.450	1	···	3	A	NGC 2068	3 Sep 2011
361	05:47:4.78	00:21:42.9	1342215587-88	096	1000.000	1	A	1080.000	1	1150.000	1	A	NGC 2068	7 Mar 2011
362	05:36:36.12	-06:38:51.9	1342227094-95	040	···	0	A	···	0	···	0	A	LDN 1641-N	22 Aug 2011
363	05:46:43.12	00:00:52.5	1342215363-64	093	25.000	1	A	29.800	1	32.100	1	A	NGC 2068	6 Mar 2011
364	05:47:36.57	00:20:6.2	1342227966-67	303	85.000	1	A	83.900	1	66.500	1	A	NGC 2068	3 Sep 2011

Table 1 continued on next page

Table 1 *(continued)*

HOPS	α_{J2000}	δ_{J2000}	OBSID[a]	Group	70μm	flag[b]	Method[c]	100μm	flag[b]	160μm	flag[b]	Method[c]	Field	Observation Date
	h:m:s	^{o} :$'$:$''$			(mJy)			(mJy)		(mJy)				(UT)
(1)	(2)	(3)	(4)	(5)	(6)	(7)	(8)	(9)	(10)	(11)	(12)	(13)	(14)	(15)
365	05:47:10.62	00:21:14.1	1342215587-88	096	34.600	1	A	52.500	1	52.800	1	A	NGC 2068	7 Mar 2011
366	05:47:3.98	00:22:10.5	1342215587-88	096	8.230	1	P	27.800	2	97.800	2	A	NGC 2068	7 Mar 2011
367	05:54:36.26	01:53:54.0	1342218778-79	004	0.082	1	A	0.061	1	0.187	1	P	LDN 1622	18 Apr 2011
368	05:35:24.72	-05:10:30.2	1342205228-29	130	110.000	1	A	81.200	1	86.200	1	A	OMC 2-3	28 Sep 2010
369	05:35:26.97	-05:10:17.1	1342205228-29	130	19.600	1	P	···	3	135.000	2	A	OMC 2-3	28 Sep 2010
370	05:35:27.63	-05:09:33.5	1342205228-29	130	824.000	1	A	702.000	1	597.000	1	A	OMC 2-3	28 Sep 2010
371	05:35:10.42	-05:55:40.9	1342204248-49	005	0.442	1	A	1.480	1	4.370	1	P	ONC-S	9 Sep 2010
372	05:41:26.34	-02:18:20.0	1342228913-14	082	6.460	1	A	16.200	1	29.900	1	A	NGC 2023-4	19 Sep 2011
373	05:46:30.68	00:02:35.3	1342215363-64	093	5.460	1	A	20.200	1	36.300	1	A	NGC 2068	6 Mar 2011
374	05:41:25.46	-07:55:18.9	1342205248-49	121	0.342	1	A	···	3	11.100	2	A	LDN 1641-S	28 Sep 2010
375	05:39:18.36	-07:20:23.6	1342227086-87	028	0.016	1	A	···	3	1.010	2	A	LDN 1641-C	22 Aug 2011
376	05:38:18.15	-07:02:26.3	1342228171-72	033	143.000	1	A	117.000	1	77.100	1	A	LDN 1641-C	4 Sep 2011
377	05:38:45.54	-07:01:2.2	1342204256-57	031	6.970	1	P	13.400	1	12.800	1	P	LDN 1641-C	10 Sep 2010
378	05:36:25.64	-06:47:16.4	1342205238-39	038	0.882	1	A	0.633	1	4.050	2	A	LDN 1641-N	28 Sep 2010
379	05:37:7.71	-06:31:57.6	1342227090-91	037	0.056	1	A	···	3	0.633	2	A	LDN 1641-N	22 Aug 2011
380	05:36:25.30	-06:25:2.6	1342205236-37	042	0.512	1	P	···	3	7.660	2	A	LDN 1641-N	28 Sep 2010
381	05:35:7.57	-05:41:54.9	1342227098-99	013	···	3	A	···	3	1.630	2	A	ONC-S	22 Aug 2011
382	05:35:21.67	-05:37:57.9	1342205234-35	015	0.132	1	A	···	3	0.347	1	A	ONC-S	28 Sep 2010
383	05:35:29.81	-04:59:51.1	1342204250-51	019	13.100	1	A	25.400	1	36.000	1	A	OMC 2-3	10 Sep 2010
384	05:41:44.09	-01:54:45.1	1342227047-48	086	993.000	1	A	914.000	1	987.000	1	A	NGC 2023-4	21 Aug 2011
385	05:46:4.77	00:14:16.3	1342205218-19	091	11.700	1	A	13.000	1	13.600	1	A	NGC 2068	28 Sep 2010
386	05:46:8.50	00:10:2.6	1342205218-19	091	24.500	1	P	54.200	1	45.100	1	P	NGC 2068	28 Sep 2010
387	05:46:7.84	00:10:0.9	1342205218-19	091	8.590	1	P	54.200	2	13.400	1	A	NGC 2068	28 Sep 2010

Table 1 continued on next page

Table 1 *(continued)*

HOPS	α_{J2000}	δ_{J2000}	OBSID[a]	Group	70μm	flag[b]	Method[c]	100μm	flag[b]	160μm	flag[b]	Method[c]	Field	Observation Date
	h:m:s	^{o} :′:″			(mJy)			(mJy)		(mJy)				(UT)
(1)	(2)	(3)	(4)	(5)	(6)	(7)	(8)	(9)	(10)	(11)	(12)	(13)	(14)	(15)
388	05:46:13.13	00:06:4.5	1342205216-17	092	32.200	1	A	35.100	1	31.200	1	A	NGC 2068	28 Sep 2010
389	05:46:47.02	00:00:27.0	1342215363-64	093	3.850	1	P	30.200	1	40.800	1	A	NGC 2068	6 Mar 2011
390	05:47:32.44	00:20:21.9	1342227966-67	303	7.700	1	A	10.700	1	14.500	1	A	NGC 2068	3 Sep 2011
391	05:47:17.06	00:20:53.3	1342215587-88	096	0.131	1	A	···	3	4.390	2	A	NGC 2068	7 Mar 2011
392	05:46:16.48	00:21:36.0	1342228374-75	302	0.120	1	A	0.235	1	0.340	1	A	NGC 2068	9 Sep 2011
393	05:46:42.48	00:23:1.3	1342218727-28	128	0.146	1	A	···	3	1.060	2	A	NGC 2068	17 Apr 2011
394	05:35:23.93	-05:07:53.5	1342205228-29	130	3.270	1	P	4.710	1	24.000	1	A	OMC 2-3	28 Sep 2010
395	05:39:17.00	-07:24:26.6	1342218729-30	026	0.100	1	A	0.622	1	2.340	1	A	LDN 1641-C	17 Apr 2011
396	05:39:13.15	-07:13:11.7	1342204252-53	029	0.037	1	A	0.263	2	0.219	1	A	LDN 1641-C	10 Sep 2010
397	05:42:48.87	-08:16:10.7	1342205254-55	061	0.687	1	A	2.020	1	4.170	1	P	LDN 1641-S	28 Sep 2010
398	05:41:29.40	-02:21:17.1	1342228913-14	082	0.392	1	A	3.000	1	8.830	1	A	NGC 2023-4	19 Sep 2011
399	05:41:24.94	-02:18:8.5	1342228913-14	082	4.690	1	A	20.400	1	50.400	1	A	NGC 2023-4	19 Sep 2011
400	05:42:45.23	-01:16:14.2	1342228376-77	090	3.440	1	A	10.900	1	16.800	1	A	NGC 2023-4	9 Sep 2011
401	05:46:7.65	00:12:20.7	1342205218-19	091	0.651	1	A	2.540	1	5.170	1	P	NGC 2068	28 Sep 2010
402	05:46:9.97	00:12:16.8	1342205218-19	091	0.414	1	A	1.980	1	4.550	1	P	NGC 2068	28 Sep 2010
403	05:46:27.75	00:00:53.8	1342215363-64	093	1.580	1	A	5.370	1	12.400	1	A	NGC 2068	6 Mar 2011
404	05:48:7.76	00:33:50.8	1342227969-70	097	1.070	1	A	4.160	1	7.720	1	A	NGC 2068	3 Sep 2011
405	05:40:58.47	-08:05:36.1	1342215361-62	066	1.730	1	A	5.790	1	10.500	1	A	LDN 1641-S	6 Mar 2011
406	05:47:43.36	00:38:22.5	1342227971-72	098	0.469	1	A	1.780	1	3.720	1	P	NGC 2068	3 Sep 2011
407	05:46:28.24	00:19:27.0	1342228374-75	302	0.386	1	P	3.100	1	6.120	1	P	NGC 2068	9 Sep 2011
408	05:39:30.75	-07:23:59.4	1342218729-30	026	0.148	1	A	0.747	1	2.150	1	A	LDN 1641-C	17 Apr 2011
409	05:35:21.40	-05:13:17.5	1342205226?27	135	13.100	1	A	32.900	1	88.900	1	A	···	···

Table 1 continued on next page

Table 1 *(continued)*

HOPS	α_{J2000}	δ_{J2000}	OBSID[a]	Group	70μm	flag[b]	Method[c]	100μm	flag[b]	160μm	flag[b]	Method[c]	Field	Observation Date
	h:m:s	^{o} :$'$:$''$			(mJy)			(mJy)		(mJy)				(UT)
(1)	(2)	(3)	(4)	(5)	(6)	(7)	(8)	(9)	(10)	(11)	(12)	(13)	(14)	(15)

[a] The unique observation identifier for Herschel.

[b] 0=erroneous designation or not observed, 1=measured, 2=upper limit, 3=not detected

[c] A=Aperture photometry, P=PSF-fitted photometry

B. APERTURE AND PSF PHOTOMETRY COMPARISON

We used both aperture and PSF photometry for all HOPS targets as described in the main text (Section 4). Figure 11 shows the comparison between the two techniques. We have additionally classified all HOPS objects as one of: (i) 'Isolated', meaning no companion or extended emission is present in the aperture or the sky annulus. (ii) 'Nearby companion or companions', meaning one or more stars may influence the photometry because of their presence in the aperture or the sky annulus. (iii) And, 'Strong background emission', meaning strong spatially extended emission from local gas and dust is detected within the aperture or the sky annulus. The classifications were made visually in the 70 μm images.

Figure 11 shows that the disagreement between the two techniques is most noticeable for sources with either companions or background emission contamination. These visual classification was used to determine which method is ultimately used for each HOPS target.

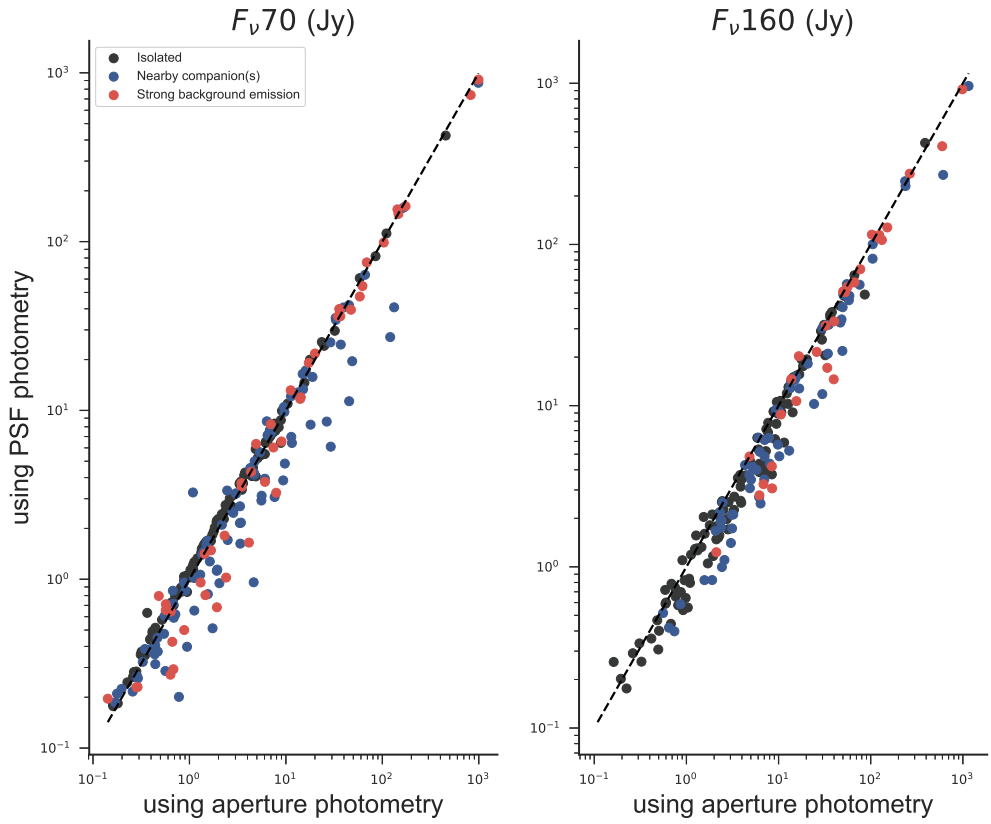

Figure 11. Comparison of photometry from the two techniques used here. The dashed line shows the trend if the two values were identical.. See text for more details on local environment classification.

REFERENCES

Adams, F., Lada, C. & Shu, F., 1987, ApJ, 312, 788

Ali, Babar, Tobin, J., J., Fischer, W. J., Poteet, C., A., Megeath, S., T., Allen, L., Hartmann, L., Calvet, N., Furlan, E. & Osorio, M., 2010, A&A, 518, L119

Konyves, V., *et al.*, 2010, A&A, 518, L106

Balog, Z., Muller, Thomas, Nielbock, Markus, Altieri, Bruno, Klass, Ulrich, Blommaert, Joris, Linz, Hendrik, Lutz, Dieter, Moor, Attila, Billot, Nicolas, Sauvage, Marc, & Okumura, Koryo, 2013, Experimental Astronomy, 38B

Cantalupo, C. M., Borrill, J. D., Jaffe, A. H., Kisner, T. S., Stompor, R. 2010 ApJS, 187, 212

Carpenter, J. M., 2000, AJ, 210, 3139

Diolaiti, Emiliano, Bendinelli, Orzio, Bonaccini, Domenico, Close, Laird, M., Currie, Douglas, G., & Parmeggiani, Gianluigi, 2000, SPIE, 4007, 879D

Dobbs, C. L., Krumholz, M. R., Ballesteros-Paredes, J., Bolatto, A. D., Fukui, Y., Heyer, M., Low, M.-M. M., Ostriker, E. C., & Vazquez-Semadeni, E. 2014, In *Protostars and Planets VI*, Henrik Beuther, Ralf S. Klessen, Cornelis P. Dullemond, and Thomas Henning (eds.), University of Arizona Press, Tucson, pp. 3-26

Draine, B. T., 2003, ARA&A, 41, 241

Dunham, M. M., Stutz, A. M., Allen, L. E., Evans, N. J., II, Fischer, W. J., Megeath, S. T., Myers, P. C., Offner, S. S. R., Poteet, C. A., Tobin, J. J. & Vorobyov, E. I. in *Protostars and Planets VI*, Henrik Beuther, Ralf S. Klessen, Cornelis P. Dullemond, and Thomas Henning (eds.), University of Arizona Press, Tucson, pp.195-218

Evans, Neal, J., II, *et al.*, 2009, ApJS, 181, 321

Feigelson, E. D., Getman, K., Townsley, L., Garmire, G., Preibisch, T., Groso, N., Montmerle, T., Muench, A., & McCaughrean, M. 2005, ApJS, 160, 379

Fischer, W., J., *et al.*, 2017, ApJ, 840, 69

Furlan, E., Fischer, W. J., Ali, B., Stutz, A. M., Stanke, T., Tobin, J. J., Megeath, S. T., Osorio, M., Hartmann, L., Calvet, N., Poteet, C.A., Booker, J., Manoj, P., Watson, D. M., & Allen, L. 2016, ApJS, 224, 5

Kennicutt, Robert, C. & Evans, Neal, J, 2012, ARA&A, 50, 531

Kryukova, E., Megeath, S., T., Hora, J., L., Gutermuth, R., A., Bontemps, S., Kraemer, K., Hennemann, M., Schneider, N., Smith, Howard, A., & Motte, F., 2014, AJ, 148, 11

McKee, C., F. & Ostriker, E., C., 2007, ARAA, 45, 565

Megeath, S. T., *et al.*, 2012, AJ, 144, 192

Lutz, D., *et al.* 2012, PACS Technical Report, PICC-ME-TN-033, http://herschel.esac.esa.int/Docs/Calibration/PACS_Point

O'Dell, C., R., Hartigan, P., Lane, W., M., Wong, S., K., Burton, M., G., Raymond, J., & Axon, D., 1997, AJ, 114, 730

Ott, S., 2010, ASP Conference Series, 434, 139

Piazzo, L., Ikhenaode, D., Natoli, P., Pestalozzi, M., Piacentini, F., & Traficante, A., 2012, IEEE Trans. on Image Processing, Vol. 21, Issue 8, pp. 3687-3696

Pilbratt, G.L., Riedinger, J.R., Passvogel, T., *et al.*, 2010, A&A, 518, L1

Poglitsch, A., Waelkens, C., Geis, N., *et al.*, 2010, A&A, 518, L2

Popesso, P., *et al.*, 2012, eprint arXiv:1211.4257

Reipurth, B. *et al.*, 2014 in PPVI, p 267.

Roussel, H., 2012, eprint arXiv:1205.2576

Schlafly, E. F., Green, G., Finkbeiner, D. P., Rix, H.-W., Bell, E. F., Burgett, W. S., Chambers, K. C., Draper, P. W., Hodapp, K. W., Kaiser, N., Magnier, E. A., Martin, N. F., Metcalfe, N., Price, P. A., & Tonry, J. L. 2014, ApJ, 786, 29

Stanke, T., *et al.*, 2015, in prep.

Stetson, P., B., 1987, PASP, 99, 191

Stutz, A., Launhardt, R., Linz, H., Krause, O., Henning, T., Kainulainen, J., Nielbock, M., Steinacker, J.,& Andre, P. 2010, A&A, 518, L87

Stutz, A., *et al.*, 2013, ApJ, 767, 36

Tegmark, M., 1997 ApJ, 480, 87

Tobin, J., J. 2015, ApJ, XX, YY

Werner, M. W., *et al.*, 2004, ApJS, 154, 1

Wieprecht, E., Schreiber, J., de Jong, J., *et al.*, 2009, ASP Conf. Ser., 411, 531